Improvements of the filtered-X algorithm in adaptive noise canceling applications

Cornelissen, D.

Award date:
1999

TECHNISCHE UNIVERSITEIT EINDHOVEN

FACULTEIT ELEKTROTECHNIEK

LEERSTOEL Signaalverwerkingssystemen

SIGNAL PROCESSING

Improvements of the filtered-X algorithm in adaptive noise canceling applications

by

Dion Cornelissen

ESM-08-99

Verslag van een afstudeeronderzoek, verricht binnen de leerstoel Signaalverwerkingssystemen onder leiding van dr.ir. P.C.W. Sommen en ing. A.C.P. van Meer in de periode november 1998 - augustus 1999

Eindhoven, augustus 1999

Improvements of the filtered-X algorithm in adaptive noise canceling applications

Dion Cornelissen (392354)
August 1999

Preface

This report describes my thesis work conducted at the Signal Processing group at the Eindhoven University of Technology. I would specially like to thank dr. Piet Sommen for guiding me through the project and for his theoretical support and Harrie van Meer because of his practical assistance.

Summary

The filtered-X algorithm is a frequently used algorithm in the field of acoustic noise canceling. This algorithm uses an estimate of the secondary path impulse response Hs to update the weights correctly. To increase the robustness of the system online adaptation of this secondary path estimate is desirable. Furthermore it is known in literature that if the phase-error between Hs and its estimate is larger than 90 degrees, for any frequency-bin, the filtered-X algorithm becomes unstable.

If the secondary path or room acoustics change, online estimation of the secondary path becomes necessary for stable filtered-X algorithm. Before the research was aimed at this online modeling of the secondary path, the properties of the acoustic noise canceller (ANC) are discussed first and used in further research. Different techniques are described and a new online modeling technique is proposed.

In this report it is shown that the reverberation characteristics of the room and the secondary path characteristics degrade the performance of the ANC. If the frequency spectrum of Hs contains frequency-bins where power is relatively low, at these frequency-bins the adaptation speed is slower and lead to a larger computational error so that the final attenuation also decreases. However if the number of loudspeakers is higher than the number of microphones, the extra secondary paths can compensate for these frequency-bins and the performance is increases significantly. This is only possible if the secondary paths don't have common frequency-bins where the power is low.

Current online adaptation techniques can be divided into two classes, namely techniques that estimate Hs by using additive noise, and overall modeling techniques without the use of additive noise. Disadvantage of the overall modeling techniques is the extra overhead that is necessary for the estimation of the primary path impulse response. Furthermore this method has difficulties when extending into a multipoint environment. The use of additive noise techniques is therefore preferred. However this method contains additive noise in the reference signal which may be audible.

In the proposed new method the noise is added to the reference signal in each frequency bin separately in such a way that its energy is low compared to the reference signal level in that bin. In this way the added noise will not significantly disturb the reference signal in an audible way. Thus only those frequency bins of Hs are updated for which the reference signal contains relatively high energy. Furthermore it is easy with this method to keep the phase error for each frequency-bin below 90 degrees. Simulation results show that with this method variations in both the primary and secondary acoustic impulse responses can be modeled in a real environment.

Contents

1. Introduction 1
1.1 Notations 1
1.2 Virtual sound sources and acoustic noise canceller 2
1.2.1 Generation of virtual sound sources 2
1.2.2 The acoustic noise canceller 4

2. The echo canceller 5
2.1. The LMS algorithm 6
2.2. Block Frequency Domain Adaptive Filtering 8
2.2.1. Explanation of BFDAF 8
2.2.2. Decorrelated LMS algorithm 10
2.3. Measurements 11
2.3.1. Measurement conditions 11
2.3.2. Influence of the reverberation on the echo-canceling 12
2.3.3. Decorrelation of input signal 16
2.3.4. Influence of unconstrained filtering 17
2.3.5. Changes of the acoustic path 18
2.4. Conclusions 19

3. The Filtered-X LMS algorithm 20
3.1. 1-1 Input-output acoustic noise canceling model 20
3.2. Derivation of the Filtered-X LMS algorithm 22
3.2.1. Effect of estimation errors on the Filtered-X LMS algorithm 24
3.3. Efficient Filtered-X BFDAF 24
3.4. Measurements and simulations 26
3.4.1. Normalization and decorrelation properties 27
3.4.2. Influence of the reverberation on the noise-canceller 28
3.4.3. Influence of the position of the secondary source 30
3.4.4. Adding loudspeakers 32
3.4.5. Effect of secondary path estimation errors 34
3.5. Conclusions 35

4. Multiple filtered-X LMS algorithm 36
4.1. Derivation of the system 36
4.2. Measurements and simulations 38
4.3. Conclusions 41

5. Online modeling of the secondary paths 42
5.1. Effect of changes in the secondary path 42
5.2. Online modeling of the secondary path 44
5.2.1. Online modeling of the delay of the secondary path 44
5.2.2. Online modeling parallel to the secondary path 45
5.2.3. Online modeling of secondary path and primary 46
5.3. Online modeling of secondary path using additive noise 47
5.3.1. Enhanced method for online modeling of the secondary path using additive noise 48
5.3.2. New online modeling technique using additive noise dependent on R 49
5.4. Conclusions 51

6. Conclusions 52
7. Future research 53

Bibliography 54

1.Introduction

This work was conducted in the Signal Processing group of the Eindhoven University of Technology. An important part of research in this group concentrates on adaptive filters and fundamental work on algorithms. Adaptive filters for acoustical and audio applications need the use of real-time implementations and large adaptive systems. These are realized on Digital Signal Processors (DSP).

This thesis project was to design and build a demonstration setup of virtual sound sources. Recent work [5, 9, 10] in the research group shows how virtual sound sources can be generated. The demonstration setup, using digital signal processors, was meant to demonstrate the possibilities of high-speed processors, in combination with digital signal processing, and making the field of signal processing more understandable to others. The virtual sound sources are developed as an application of the acoustic noise canceller.

The theoretical approach of the virtual sound source is based on the acoustic noise canceller (ANC). In section 1.2.1, the basic principle of generating a virtual sound source is described, while the relation between a virtual sound source and ANC is discussed in section 1.2.2. In the next chapters the ACN is described thoroughly. The generation of virtual sound sources is only used as an example application and is not realized.

In chapter 2 the echo canceller is discussed and in chapter 3 this echo canceller is extended to the single-input-single-output (1-1) ANC and the 1-2 input-output ANC. The filtered-X algorithm is used as an algorithm for the ANC. The advantages of the 1-2 input-output ANC compared to the 1-1 input-output ANC are discussed in this chapter. In chapter 4 the 2-2 input-output ANC is described. The convergence properties of the echo-canceller are discussed in chapter 2 and for the ANC in chapter 3 and 4. The filtered-X algorithm requires an accurate estimate of the secondary path for stable filtering, therefor online secondary path modeling techniques are desired if the secondary path can change. These online modeling techniques are discussed in chapter 5.

1.1 Notations

In this report, upper-case characters are used for frequency domain and lower-case characters for time domain signals. Furthermore, boldface characters are used for diagonal matrices and underlined boldface characters for vectors, e.g. $\mathbf{H} = diag\{\underline{\mathbf{H}}\}$. The transformation of a vector to a diagonal matrix is used to provide the correct calculations.

The only exception is the Fourier matrix $\mathbf{F}_N$ that has elements of the form $e^{-j\frac{2\pi}{N}nm}$, with N the transformation length. For example: $\underline{\mathbf{H}} = \mathbf{F} \cdot \underline{\mathbf{h}}$, with $\underline{\mathbf{H}} = (H_0, H_1,..H_{N-1})^t$ and $\underline{\mathbf{h}} = (h[k], h[k-1],..h[k-N+1])^t$, where $(.)^t$ denotes the transpose.

1.2 Virtual sound sources and acoustic noise canceller

1.2.1 Generation of virtual sound sources

In a normal two-loudspeaker stereo-setup a listener will localize sounds that are produced by those loudspeakers as coming from between those loudspeakers. If those two loudspeakers are very close (e.g. in a TV) all sounds are perceived as coming out of the TV. This is not desired because the stereo effect decreases. In an ideal situation sounds are localized by a listener as coming from an arbitrary point in a room without changing the positions of the loudspeakers. This is possible if the input signals of the loudspeakers are altered such that the sounds are localized by a listener as coming from an arbitrary point in the room. Such a point is called a virtual sound source because this sound source is not physically available, but is created at that point using real sound sources at other points. The virtual sound sources can be generated if the signals that drive the loudspeakers are filtered correctly, this means that the two loudspeakers produce the same sound pressures on the ears of a listener as a sound source on a virtual point produces. The sound pressures on the ears are measured with microphones and converted to signals.

In a normal stereo-setup 2 loudspeakers are available. With these two loudspeakers a virtual sound source is created for 1 listener while the listener has 2 ears to localize the sound source.

Mathematically the filters that drive the loudspeakers can be described easily, but the implementation of the filters is more difficult as will be explained in the next chapters. Equations for the sound pressures on the ears of a listener can be derived using figure 1.1. In this figure the input signal $x[k]$ is directly connected to the loudspeaker at the virtual point L_p, the signals that drive both loudspeakers L_l and L_r are respectively filtered with impulse responses $\underline{\mathbf{w}}_l$ and $\underline{\mathbf{w}}_r$. The sound pressures at both microphones (M_l and M_r at the position of a listener ears) are measured and converted to respectively $r_l[k]$ and $r_r[k]$.

Furtheron the loudspeaker at the virtual point L_p is called the primary sound source and the loudspeakers L_r and L_l are called the secondary sound sources. By this the transfer functions $\underline{\mathbf{h}}_{pl}$ and $\underline{\mathbf{h}}_{pr}$ are the primary paths and $\underline{\mathbf{h}}_{ll}$, $\underline{\mathbf{h}}_{rl}$, $\underline{\mathbf{h}}_{lr}$ and $\underline{\mathbf{h}}_{rr}$ are the secondary paths. $\underline{\mathbf{h}}_{pl}$ is the transfer function from primary source L_p to the left microphone M_l, ditto for $\underline{\mathbf{h}}_{pr}$. $\underline{\mathbf{h}}_{ll}$ is the transfer function from left secondary sound source L_l to the left microphone M_l, ditto for $\underline{\mathbf{h}}_{rl}$, $\underline{\mathbf{h}}_{lr}$ and $\underline{\mathbf{h}}_{rr}$. These primary and secondary paths not only describe the acoustical transfer functions from loudspeaker to microphone, but also the non-idealities of D/A and A/D-converters and non-linearity's of loudspeakers and microphone (-amplifiers).

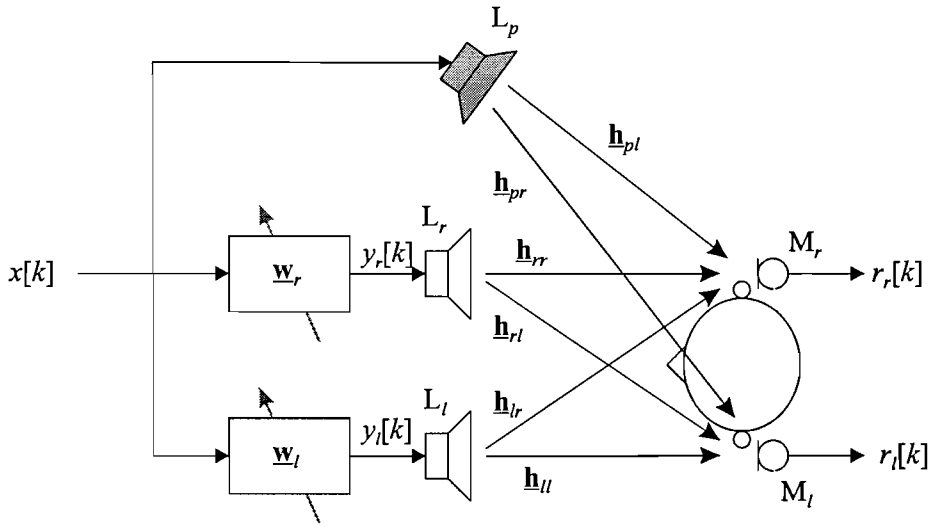

Figure 1.1. Virtual sound source setup

The measured signals $r_r[k]$ and $r_l[k]$ can be separated in two parts: one part is produced by the primary source and one part is produced by the secondary sources. Both parts can be described in frequency domain by:

$$\underline{\mathbf{R}}_{ls} = \mathbf{X} \cdot \mathbf{H}_{ll} \cdot \underline{\mathbf{W}}_l + \mathbf{X} \cdot \mathbf{H}_{rl} \cdot \underline{\mathbf{W}}_r \qquad (1.1)$$

$$\underline{\mathbf{R}}_{rs} = \mathbf{X} \cdot \mathbf{H}_{lr} \cdot \underline{\mathbf{W}}_l + \mathbf{X} \cdot \mathbf{H}_{rr} \cdot \underline{\mathbf{W}}_r \qquad (1.2)$$

as a function of the secondary sources (L_l and L_r), and

$$\underline{\mathbf{R}}_{lp} = \mathbf{X} \cdot \underline{\mathbf{H}}_{pl} \qquad (1.3)$$

$$\mathbf{R}_{rp} = \mathbf{X} \cdot \underline{\mathbf{H}}_{pr} \qquad (1.4)$$

as a function of the primary source (L_p). In the case of a virtual sound source generator this leads to: $\underline{\mathbf{R}}_{lp} = \underline{\mathbf{R}}_{ls}$ and $\underline{\mathbf{R}}_{rp} = \underline{\mathbf{R}}_{rs}$, because the sound pressures measured on both ears coming from the secondary sources are equal to the sound pressures produced by the primary sound source. Combining equations (1.1), (1.2), (1.3) and (1.4) results in:

$$\underline{\mathbf{H}}_{pl} = \mathbf{H}_{ll} \cdot \underline{\mathbf{W}}_l + \mathbf{H}_{rl} \cdot \underline{\mathbf{W}}_r, \qquad (1.5)$$

$$\underline{\mathbf{H}}_{pr} = \mathbf{H}_{lr} \cdot \underline{\mathbf{W}}_l + \mathbf{H}_{rr} \cdot \underline{\mathbf{W}}_r. \qquad (1.6)$$

These formulas can easily be rewritten as:

$$\underline{\mathbf{H}}_p = \mathbf{H}_s \cdot \underline{\mathbf{W}}_{VIRT}, \qquad (1.7)$$

with $\underline{\mathbf{H}}_p = \begin{pmatrix} \underline{\mathbf{H}}_{pl} \\ \underline{\mathbf{H}}_{pr} \end{pmatrix}$, $\mathbf{H}_s = \begin{pmatrix} \mathbf{H}_{ll} & \mathbf{H}_{rl} \\ \mathbf{H}_{lr} & \mathbf{H}_{rr} \end{pmatrix}$ and $\underline{\mathbf{W}}_{VIRT} = \begin{pmatrix} \underline{\mathbf{W}}_l \\ \underline{\mathbf{W}}_r \end{pmatrix}$.

Solving equations (1.5), (1.6) and (1.7) leads to:

$$\underline{\mathbf{W}}_l = \frac{\mathbf{H}_{rr} \cdot \underline{\mathbf{H}}_{pl} - \mathbf{H}_{rl} \cdot \underline{\mathbf{H}}_{pr}}{\mathbf{H}_{ll} \cdot \mathbf{H}_{rr} - \mathbf{H}_{lr} \cdot \mathbf{H}_{rl}}, \qquad (1.8)$$

$$\underline{\mathbf{W}}_r = \frac{\mathbf{H}_{lr} \cdot \underline{\mathbf{H}}_{pl} - \mathbf{H}_{rr} \cdot \underline{\mathbf{H}}_{pr}}{\mathbf{H}_{ll} \cdot \mathbf{H}_{rr} - \mathbf{H}_{lr} \cdot \mathbf{H}_{rl}}, \qquad (1.9)$$

or equivalently: $$\underline{\mathbf{W}}_{VIRT} = \mathbf{H}_s^{-1} \cdot \underline{\mathbf{H}}_p . \qquad (1.10)$$

This means that all transfer functions $\underline{\mathbf{H}}_{pl}$, $\underline{\mathbf{H}}_{pr}$, $\mathbf{H}_{ll}$, $\mathbf{H}_{rr}$, $\mathbf{H}_{rl}$ and $\mathbf{H}_{lr}$ are necessary to calculate the filters $\underline{\mathbf{W}}_l$ and $\underline{\mathbf{W}}_r$. Because small movements of the head of a listener will change all transfer functions and thus introduce errors, adaptive filters are required to update the transfer functions and calculate new values for $\underline{\mathbf{W}}_l$ and $\underline{\mathbf{W}}_r$.

If the filters $\underline{\mathbf{W}}_l$ and $\underline{\mathbf{W}}_r$, as calculated in (1.10), are implemented in the filters that drive the secondary sources, the same sound pressures on the ears are produced by the secondary sound sources as the primary source that is driven by the same signal would produce. This means that with the secondary sound sources a virtual sound source is created on the position of the primary source (see figure 1.1).

The filters $\underline{\mathbf{W}}_l$ and $\underline{\mathbf{W}}_r$ are not calculated using equation (1.10), but are obtained using an acoustic noise canceller. The acoustic noise canceller is used to cancel sounds, often noise, produced by a primary source or loudspeaker at the position of the virtual sound source. The acoustic noise canceller uses adaptive filters to obtain $-\underline{\mathbf{W}}_l$ and $-\underline{\mathbf{W}}_r$, as will be discussed in section 1.2.2. Next step is to shut off the primary loudspeaker. The secondary loudspeakers are now driven by the input signal filtered by $\underline{\mathbf{W}}_l$ and $\underline{\mathbf{W}}_r$. A listener now interprets the sounds as coming from the primary sound source. This is called virtual sound source, because the primary sound source does not generate any sounds, all sounds are produced by the secondary sound sources.

1.2.2 The acoustic noise canceller

The principle of the virtual sound source is based on the Acoustic Noise Canceller (ANC). The ANC is used to cancel undesired sounds, often noise, in the ears of a listener or in microphones by generating anti sound. The noise is produced by the primary sound source and the secondary sound sources are used to delete this disturbing noise on the ears of a listener. The main difference between the virtual sound source and the ANC is that the ANC cancels the sounds from a primary source, and the virtual sound source generates the same sounds as the primary source. In case of the ANC this leads to: $\underline{\mathbf{R}}_{lp} = -\underline{\mathbf{R}}_{ls}$ and $\underline{\mathbf{R}}_{rp} = -\underline{\mathbf{R}}_{rs}$, this means that equations (1.7) and (1.10) can be written as:

$$\mathbf{H}_p = -\mathbf{H}_s \cdot \underline{\mathbf{W}}_{ANC}, \text{ and} \qquad (1.11)$$

$$\underline{\mathbf{W}}_{ANC} = -\mathbf{H}_s^{-1} \cdot \underline{\mathbf{H}}_p, \qquad (1.12)$$

with $\underline{\mathbf{W}}_{ANC} = \begin{pmatrix} \underline{\mathbf{W}}_l \\ \underline{\mathbf{W}}_r \end{pmatrix}$. Thus, the transfer functions of the ANC filters are the exact opposite of the transfer functions of the virtual sound source filters:

$$\underline{\mathbf{W}}_{VIRT} = -\underline{\mathbf{W}}_{ANC} \qquad (1.13)$$

The main disadvantage of the system is that the filters, $\underline{\mathbf{W}}_l$ and $\underline{\mathbf{W}}_r$, only hold for one position in the room. For every new point the new filters have to be calculated. Adaptive filters are therefore desired [20]. An introduction to adaptive filters is given in chapter 2, and in chapter 3 the filtered-X method is presented to obtain the filters $\underline{\mathbf{W}}_l$ and $\underline{\mathbf{W}}_r$ using adaptive filters.

2. The echo canceller

Chapter one described the main disadvantage of the ANC namely that the system is only valid for one position of a listener. An adaptive ANC is desired so that acoustic noise canceling is also possible in other or changing positions in the room, an adaptive ANC is able to track these variations [5]. This chapter deals with the implementation of adaptive filters and an application of these adaptive filters, the so-called echo canceller, is discussed. In the next chapter will be discussed how this acoustic echo-canceller can be converted to an ANC.

An acoustic echo canceller is used when a sound signal is distorted with an echo, or noise, and *a priori* knowledge of this echo is available. For example in an audio conferencing application, see figure 2.1. Audio conferencing is a setup where people at different locations try to communicate with each other using a system of microphones and loudspeakers. The main problem in audio conferencing is that if a person in the left room talks, he will hear an undesirable echo. This is because the sound signal $x[k]$, received by microphone M_l from this person, is transmitted via the right loudspeaker L_r (in the right room) back into the microphone M_r. The signal $d[k]$ returns to that person trough the left loudspeaker L_l. The signal $d[k]$ contains an undesired acoustic echo $d_1[k]$ and a desired audio signal $d_2[k]$ from the right person. The undesired echo is produced by the right loudspeaker L_r and picked up by the microphone M_r with an acoustical impulse response $\underline{\mathbf{h}}_{ref}$. This echo is unwanted and it is therefore desired to cancel this echo using an adaptive filter, before it returns to the left room. Adaptive filters are preferred because the acoustic path can change. Thus, in an ideal situation the echo is fully cancelled and only the desired signal $d_2[k]$ is transmitted to the loudspeaker in the left room L_l.

In section 2.1, the Least Mean Square algorithm (LMS) will be used as an adaptive filter. An efficient LMS-algorithm, the Block Frequency Domain Adaptive Filter (BFDAF) is described in section 2.2. The convergence speed and the final error of this adaptive echo-canceller will be examined with some experiments in section 2.3.

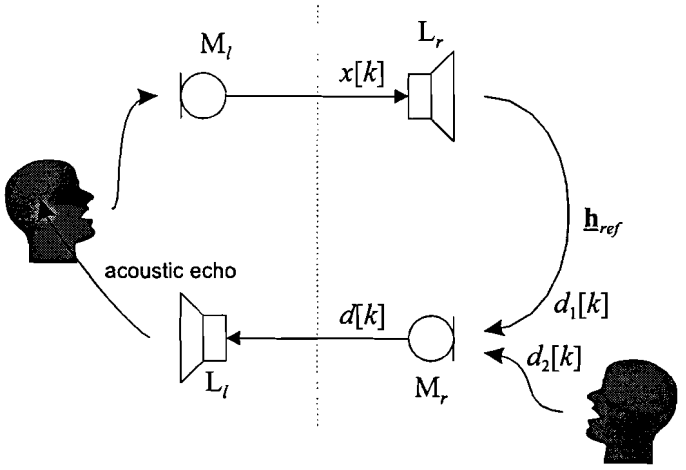

Figure 2.1. The audio conferencing problem

2.1. The LMS algorithm

With the audio conferencing setup we have seen that the existing echo signal, $d_1[k]$, in $d[k]$ is undesired, and must be cancelled using *a priori* information. Because signal $x[k]$ is known, *a priori* information of the echo is available. The adaptive filter has to delete the echo $d_1[k]$ in $d[k]$, and only the desired signal $d_2[k]$ has to be transmitted to L_l. By deleting an estimate of $d_1[k]$ from the signal $d[k]$ this can be done. The Least Mean Squares (LMS) algorithm is an adaptive algorithm that obtains an estimate of an unknown transfer function or impulse response by minimizing the Mean Squared Error (MSE) (see figure 2.2). We can also say that all correlation between $d[k]$ and $x[k]$ is minimized.

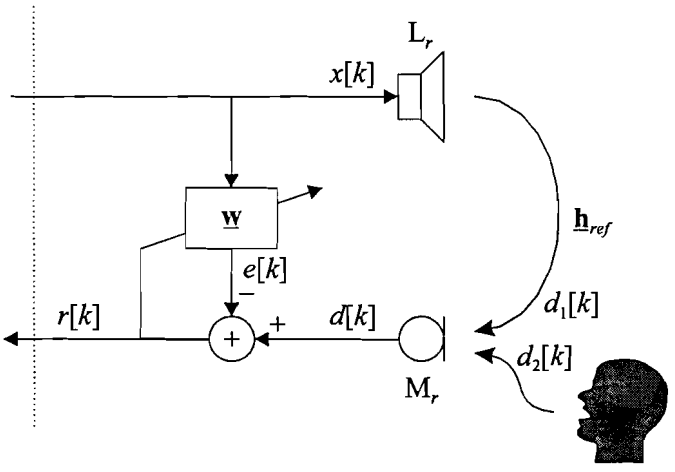

Figure 2.2. Adaptive filter diagram

An unknown transfer function, with impulse response $\underline{\mathbf{h}}_{ref}$, and the adaptive filter $\underline{\mathbf{w}}$, are driven by the same input signal $x[k]$, see figure 2.2. The reference signal consists of 2 parts, $d[k] = d_1[k] + d_2[k]$, with $d_1[k]$ the output signal of the unknown filter that is correlated with the input signal $x[k]$. Signal $d_2[k]$ is uncorrelated with $x[k]$ and is often a desired signal. The error signal is defined by

$r[k] = d[k] - e[k]$. To estimate $\underline{\mathbf{h}}_{ref}$ by $\underline{\mathbf{w}}$ it is nessecary to minimize the mean squared error $E\{r^2[k]\}$, with $E\{..\}$ the mathematical expectation operator. The MSE can be written as

$$E\{r^2[k]\} = E\{(d_1[k] + d_2[k] - e[k])^2\} = E\{(d_1[k] - e[k])^2\} + E\{d_2^2[k]\} \qquad (2.1)$$

The right side of equation (2.1) can be split because $d_2[k]$ is not correlated with $d_1[k]$ and $e[k]$. The optimal solution is when the power of the error signal is minimal, in this case $d_1[k] \approx e[k]$. Then holds also $\underline{\mathbf{h}}_{ref} \approx \underline{\mathbf{w}}$ and $r[k] \approx d_2[k]$.

Using a FIR-filter, like a tapped-delay-line, $e[k]$ can be written as a convolution between the input signal and the filter coefficients:

$$e[k] = \sum_{i=0}^{M-1} w_i[k] \cdot x[k-i] = \mathbf{x}_M'[k] \cdot \underline{\mathbf{w}}_M[k] \qquad (2.2)$$

with M the number of filter coefficients, $\mathbf{x}_M[k] = (x[k-M+1],...,x[k-1],x[k])'$ and $\underline{\mathbf{w}}_M[k] = (w_{M-1}[k],...,w_1[k],w_0[k])'$. In general $d_1[k]$ can be written as a convolution of the input signal $x[k]$ and the 'infinite' acoustical transfer function $\underline{\mathbf{h}}_{ref}$:

$$d_1[k] = \sum_{i=0}^{\infty} h_{ref,i}[k] \cdot x[k-i] = \underline{\mathbf{x}}'[k] \cdot \underline{\mathbf{h}}_{ref}[k] \qquad (2.3)$$

To minimize $E\{r^2[k]\}$ it is necessary that the gradient with respect to $\underline{\mathbf{w}}_M[k]$ is zero:

$$\min E\{r^2[k]\} \Rightarrow \frac{\partial E\{r^2[k]\}}{\partial \underline{\mathbf{w}}_M[k]} = \nabla_M = 2E\left\{r[k] \cdot \frac{\partial r[k]}{\partial \underline{\mathbf{w}}_M[k]}\right\} = -2E\{r[k] \cdot \mathbf{x}_M[k]\} = \underline{0} \qquad (2.4)$$

The optimal weight vector then becomes:

$$E\{d_1[k] \cdot \mathbf{x}_M[k]\} = E\{\mathbf{x}_M[k] \cdot \mathbf{x}_M'[k]\} \cdot \underline{\mathbf{w}}_M[k] \Rightarrow \underline{\mathbf{p}} = \mathbf{R}_x \cdot \underline{\mathbf{w}}_M \Rightarrow \underline{\mathbf{w}}_M = \mathbf{R}_x^{-1} \cdot \underline{\mathbf{p}}. \qquad (2.5)$$

With $\mathbf{R}_x$ the autocorrelation matrix of the input signal and $\underline{\mathbf{p}}$ the cross-correlation vector between input signal $x[k]$ and $d_1[k]$.

The update equation is obtained using an instantaneous estimate of the gradient (equation (2.4)):

$$\underline{\mathbf{w}}_M[k+1] = \underline{\mathbf{w}}_M[k] - \alpha \cdot \nabla_M \approx \underline{\mathbf{w}}_M[k] + 2 \cdot \alpha \cdot r[k] \cdot \mathbf{x}_M[k] \qquad (2.6)$$

with α the adaptation constant. We use an instantaneous estimate of the expectation $E\{r[k] \cdot \mathbf{x}_M[k]\} \approx r[k] \cdot \mathbf{x}_M[k]$ in the update of the LMS algorithm.

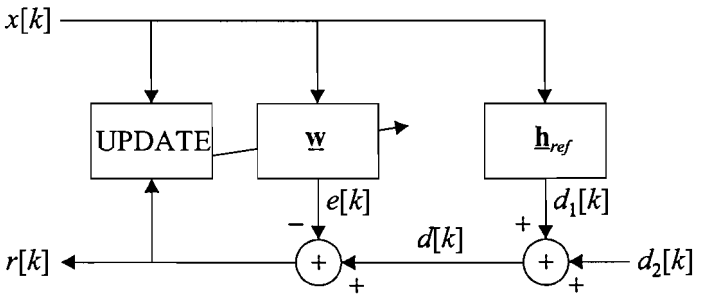

Figure 2.3. Adaptive filter diagram

Because the power of the output signal $r[k]$ is directly influenced by the power of the input signal $x[k]$ it follows that the quantity of $E\{r[k]\cdot \mathbf{x}_M[k]\}$ depends on $E\{\mathbf{x}'_M[k]\cdot \mathbf{x}_M[k]\} = \sigma_x^2[k]$. The adaptation process is thus directly dependent on the input signal variance. To make the adaptation less dependent of the input signal, normalization of the adaptation constant $\alpha/\hat{\sigma}_x^2[k]$ is used, with $\hat{\sigma}_x^2[k]$ an estimate of σ_x^2. This leads to the Normalized-LMS (NLMS) algorithm:

$$\underline{\mathbf{w}}_M[k+1] = \underline{\mathbf{w}}_M[k] + 2\cdot\frac{\alpha}{\hat{\sigma}_x^2[k]}\cdot r[k]\cdot \mathbf{x}_M[k] \qquad (2.7)$$

For the estimate $\hat{\sigma}_x^2[k]$ we use:

$$\hat{\sigma}_x^2[k] = \beta\cdot\hat{\sigma}_x^2[k-1] + (1-\beta)\cdot x^2[k], \text{ with } 0<\beta<1. \qquad (2.8)$$

2.2. Block Frequency Domain Adaptive Filtering

In the previous section we have seen that the update equation (2.6) and the calculation of $e[k]$ (2.2) requires a correlation respectively a convolution operation. For large filter lengths a convolution and a correlation operation are more efficiently calculated in frequency domain than in time domain, because both operations are converted into elements-wise multiplication's. So, in order to reduce complexity of the adaptive filter, the filter is realized in frequency-domain resulting in the so-called Block-Frequency Domain Adaptive Filter (BFDAF) [15]. Not only the convolution and the correlation operation are calculated in frequency domain, all operations take place in frequency domain. This means that blocks of time samples are transformed to frequency domain samples using a Discrete Fourier Transform (DFT).

The main advantages of the BFDAF, with respect to the time domain implementation, are:
- BFDAF uses a block-by block update algorithm to reduce complexity. Therefore the update of the filter coefficients takes place after each block.
- The correlation and convolution operations are more efficient in frequency than in time-domain.
- In time-domain all input samples are correlated with each other, using a DFT leads to a much more uncorrelated system. Different stepsizes can be used for different frequency-bins to increase convergence speed.

The Fast Fourier Transform (FFT) is used as an efficient implementation of the DFT. Because the calculation time of the FFT/IFFT's is much longer than the other calculations, the number of FFT/IFFT's approximates the total calculation time of the BFDAF system.

2.2.1. Explanation of BFDAF

The explanation of the BFDAF is given in [15], a short and brief overview will be given below.

The input signal $x[k]$ of the LMS algorithm is used in a convolution with the filter coefficients $\underline{\mathbf{w}}_M[k]$ to calculate $e[k]$. The convolution operator in time-domain is replaced by an elements-wise multiplication in the frequency domain, this reduces the number of calculation operations significantly. A DFT is used to calculate the frequency samples of the input signal and the filter

coefficients. Problem is that an elements-wise multiplication in frequency domain performs a cyclic operation in time domain where a linear operation is needed. A linear operation is possible if an overlap-save method is used. This method uses a vector of B input samples $\underline{\mathbf{x}}_B[kL]$ and a filter $\underline{\mathbf{w}}_M[kL]$ of length M. With B=L+M-1, this method produces L correct output samples $\underline{\mathbf{e}}_L[kL]$.

This means that in each block a set of L new input samples $x[k]$ are used, with $L \geq 1$, because only L correct output samples are calculated. Combining a block of L new samples $\mathbf{x}_L[kL] = (x[k-L+1],..,x[k-1],x[k])^t$ and M-1 previous time samples results in the necessary blocklength B, $\mathbf{x}_B[kL] = (x[k-B+1],..,x[k-1],x[k])^t$. Via the DFT a vector of frequency samples is calculated

$$\mathbf{X}_B[kL] = \mathbf{F}_B \cdot \mathbf{x}_B[kL]. \tag{2.9}$$

With $\mathbf{F}_B$ the (B×B) Fourier matrix, $\mathbf{X}_B[kL] = \{X_0, X_1,.., X_{B-1}\}$. $\underline{\mathbf{W}}_B[kL]$ is calculated using a DFT of the filter $\underline{\mathbf{w}}_M[kL]$, padded with L-1 zeros, this results in

$$\underline{\mathbf{W}}_B[kL] = \mathbf{F}_B \cdot \begin{pmatrix} \mathbf{0}_{L-1} \\ \underline{\mathbf{w}}_M[kL] \end{pmatrix}. \tag{2.10}$$

Elements-wise multiplication of $\underline{\mathbf{X}}_B[kL]$ with $\underline{\mathbf{W}}_B[kL]$ leads to

$$\underline{\mathbf{E}}_B[kL] = \underline{\mathbf{X}}_B[kL] \otimes \underline{\mathbf{W}}_B[kL]. \tag{2.11}$$

After an inverse DFT the correct L output samples $\underline{\mathbf{e}}_L[kL]$ are available:

$$\underline{\mathbf{e}}_L[kL] = \begin{pmatrix} \mathbf{0}_{M-1,L} & \mathbf{I}_{L,L} \end{pmatrix} \cdot \mathbf{F}_B^{-1} \cdot \underline{\mathbf{E}}_B[kL]. \tag{2.12}$$

with $\mathbf{0}_{M\text{-}1,L}$ the (M-1×L) zero matrix and $\mathbf{I}_{L,L}$ the (L×L) identity matrix.

For the update of the adaptive filter $\underline{\mathbf{w}}_M[k]$ a correlation operation of the input signal $x[k]$ with the error signal $r[k]$ is necessary (equation (2.6)). This correlation is described, just like the convolution operation, in frequency domain because of efficiency reasons. The main difference between the convolution and correlation operation in frequency domain is the conjugate of the input block. The approximation of the gradient can be calculated as an elements-wise multiplication of $\underline{\mathbf{X}}_B^*[kL]$ and $\underline{\mathbf{R}}_B[kL]$:

$$\underline{\nabla}_B[kL] = \underline{\mathbf{X}}_B^*[kL] \otimes \underline{\mathbf{R}}_B[kL] \tag{2.13}$$

The update equation of the filter $\underline{\mathbf{W}}_B[kL]$ can now be written as:

$$\underline{\mathbf{W}}_B[(k+1)L] = \underline{\mathbf{W}}_B[kL] + \frac{2\alpha}{L} \cdot \mathbf{G} \cdot \underline{\nabla}_B[kL] \tag{2.14}$$

for the LMS-algorithm. The factor 1/L is coming from the block of L input samples. The matrix $\mathbf{G} = \mathbf{F}_B \cdot \begin{pmatrix} \mathbf{0}_{L-1,L-1} & \mathbf{0}_{L-1,M} \\ \mathbf{0}_{M,L-1} & \mathbf{I}_{M,M} \end{pmatrix} \cdot \mathbf{F}_B^{-1}$ is used because only the M correct gradient samples are used in the update of $\underline{\mathbf{W}}_B[kL]$. This is called constrained filtering. The correct gradient samples in time domain are calculated with an inverse DFT, and then padded with zeros to calculate the correct gradient in frequency domain using the DFT. Furthermore $\mathbf{0}_{A,B}$ is the (A×B) zero matrix and $\mathbf{I}_{M,M}$ the (M×M) identity matrix. Leaving out this operation is called unconstrained filtering and decreases the total number of FFT/IFFT's by 2, and thus decreases the calculating time. In [5] it was stated that the

leaving out this operation increases the maximal attenuation because it 'increases' the filter length. It also leads to a wrap-around error and this is not desired.

Converting the input samples from serial to parallel has as consequence that there is a processing delay of L samples, d_L. This all results in the BFDAF system of figure 2.4.

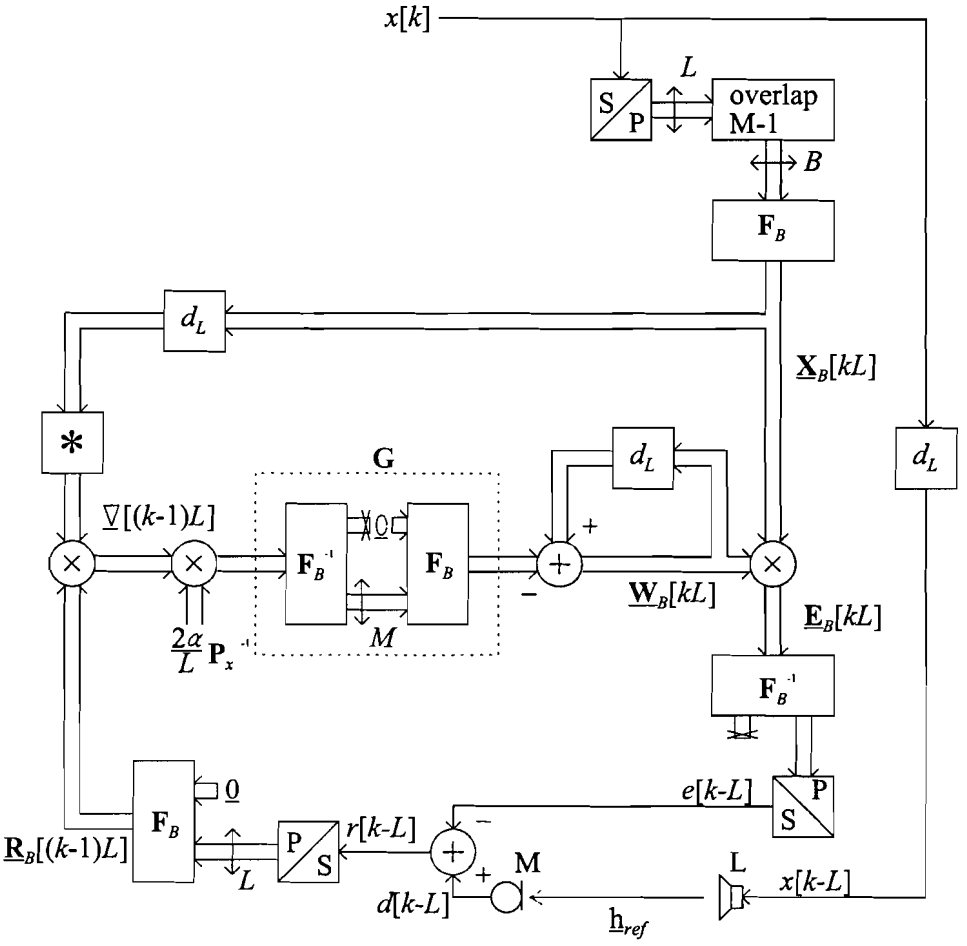

Figure 2.4. Block Frequency Domain Adaptive Filter

2.2.2. Decorrelated LMS algorithm

In section 2.1 was discussed that the statistics of the input signal influence the adaptation process. To make the adaptation process independent on the input signal statistics decorrelation of the input signal performs well. This leads to the decorrelated LMS algorithm:

$$\underline{\mathbf{W}}_B[(k+1)L] = \underline{\mathbf{W}}_B[kL] + \frac{2\alpha}{L} \cdot \mathbf{G} \cdot \mathbf{P}_x^{-1} \cdot \underline{\nabla}_B[kL] \qquad (2.15)$$

The diagonal matrix $\mathbf{P}_x$ represents the power spectrum of the input signal. An estimate of this power spectrum is calculated with

$$\mathbf{P}_x[kL] = \beta \cdot \mathbf{P}_x[(k-1)L] + (1-\beta) \cdot \left(\mathbf{X}^*[kL] \cdot \mathbf{X}[kL]\right), \text{ with } 0 < \beta < 1. \qquad (2.16)$$

2.3. Measurements

In this section some important properties that describe the quality of the echo-canceller are discussed. First, the influence of reverberation in a room on the adaptation will be described in section 2.3.2 and second, the influence of the correlation of the input signal in section 2.3.3. We will see that the correlation of the input signal determines the speed of convergence, while the reverberation, in combination with the number of filter coefficients, determine the maximum possible echo-cancellation.

In section 2.3.4 the effect of unconstrained filtering, as discussed in section 2.2.1, will be discussed and in section 2.3.5 the adaptation of the echo-canceller to a change in the acoustic path is discussed.

2.3.1. Measurement conditions

This section describes the measurement conditions. All measurements are performed in an empty office room with room dimensions L×W×H = 4.90 m × 4.80 m × 3.10 m.

The adaptation plot is measured using the following setup:
- A white noise signal will be used as an input signal.
- The sampling frequency is 8 kHz.
- The distance between loudspeaker and microphone is 100 cm.
- The room is empty, no curtains on the walls, one side of the room has windows and the other sides are walls.
- The blocklength B=4096 samples, the number of new samples L=2048, the filter length is thus M=2049 samples.

The maximal echo-cancellation can be calculated using the adaptation plot, figure 2.5. The adaptation plot gives the Mean Squared Error (MSE) as a function of time. An estimate of the MSE is calculated using L samples of the error signal $r[k]$:

$$E\{r^2[kL]\} \approx \frac{\sum_{i=0}^{L-1} r^2[kL-i]}{L} \qquad (2.17)$$

The attenuation can be calculated as follows:

$$Att = E\{r^2[kL]\} / E\{d^2[kL]\} \qquad (2.18)$$

$E\{d^2[kL]\}$ is measured if no adaptation is used, in this case $E\{r^2[kL]\} = E\{d^2[kL]\}$.

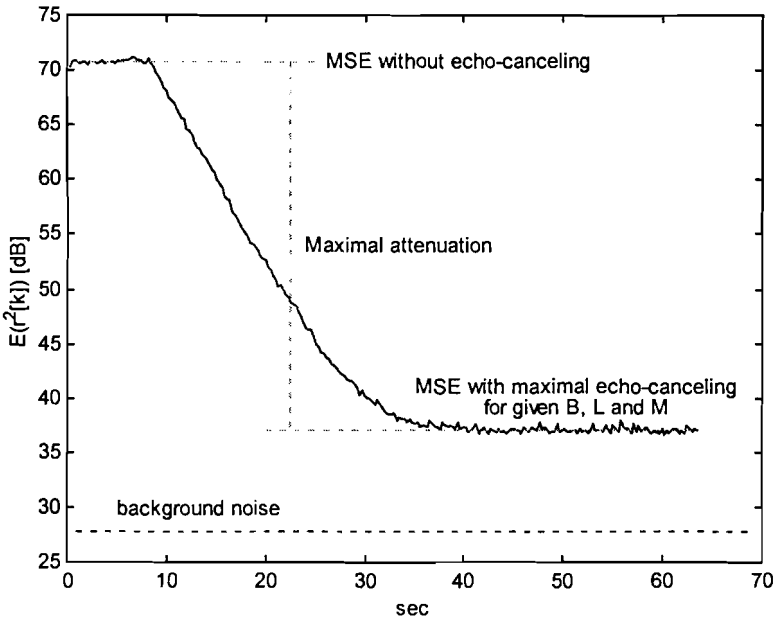

Figure 2.5. Adaptation plot, B=4096, L=2048 and M=2049.

The duration of this measurement is 64 seconds. The first 8 seconds no adaptation is performed, this is done to measure $E\{d^2[kL]\}$, in this case MSE=70.8 dB. After 8 seconds the adaptation starts and the final MSE is here reached after 40 seconds. The MSE with maximal echo canceling can now be measured, 37.1 dB. The difference between the MSE without and the MSE with echo canceling is the maximal attenuation, 33.7 dB. The background noise is measured 27.8 dB to determine the maximal possible attenuation, the maximal possible attenuation is 70.8 dB - 27.8 dB = 43.0 dB.

2.3.2. Influence of the reverberation on the echo-canceling

The reverberation time is a measure for the duration of the impulse response in a room. If the reverberation time is long the duration of the impulse response will be long. The reverberation time is the time in which the sound pressure level decreases by 60 dB. In normal office rooms, a reverberation time of 0.5 sec is normal. In very reverberant rooms, for example a church, the reverberation can be much longer, about 1.4-1.6 sec.

The reverberation time depends on the dimensions of the room and the absorption coefficients of the walls, the floor and the ceiling of the room. The larger the absorption coefficients of the room, the smaller the reverberation time, because more sound power is absorbed. The reverberation time is independent on the position of a loudspeaker or microphone.

For the determination of the reverberation time the reverberation curve $T(p)$ is used. This reverberation curve can be written as follows:

$$T(p) = \frac{\sum_{i=p}^{\infty} h_{ref,i}^2}{\sum_{i=0}^{\infty} h_{ref,i}^2} \qquad (2.19)$$

This curve plots the residual sound power, $\sum_{i=p}^{\infty} h_{ref,i}^2$, in proportion to the total sound power $\sum_{i=0}^{\infty} h_{ref,i}^2$ as a function of time.

In this section a couple of measurements will be performed to show the influence of the reverberation time on the echo canceling. The following setup is used:

- A white noise signal is used as an input signal.
- The sampling frequency is 8 kHz.
- The distance between loudspeaker and microphone is 100 cm.
- The room is empty, no curtains on the walls, one side of the room has windows and the other sides are walls.

First, the unknown impulse response $\underline{\mathbf{h}}_{ref}$ is estimated using the LMS-algorithm. The blocklength B=4096 samples, the number of new samples L=1024, the filter length M=3073 samples. The LMS algorithm is used to estimate the unknown impulse response $\underline{\mathbf{h}}_{ref}$. The estimated impulse response is given in figure 2.6. The related frequency response is in figure 2.7. Note that for low and high frequencies the magnitude of $\underline{\mathbf{H}}_{ref}$ is strongly attenuated. The attenuation of the high frequencies is due to the A/D and D/A-converter and the attenuation of the low frequencies is due to the microphone's input amplifier. For the frequencies between 350 and 3300 Hz the acoustical path from loudspeaker to microphone is responsible. The phase plot is almost linear, the D/A and A/D converters degrade the phase for the high frequencies. If the impulse response is a pure delay the phase plot is linear.

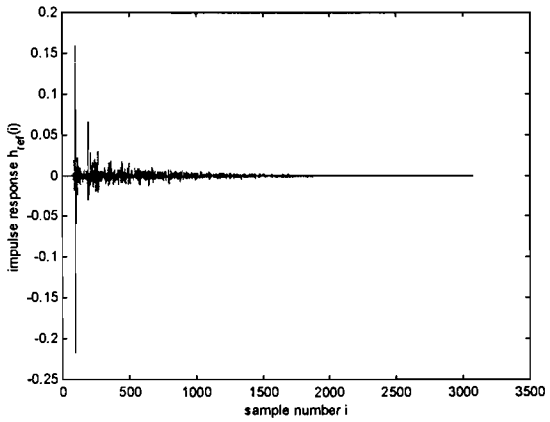

Figure 2.6. Estimated impulse response $\underline{\mathbf{h}}_{ref}$

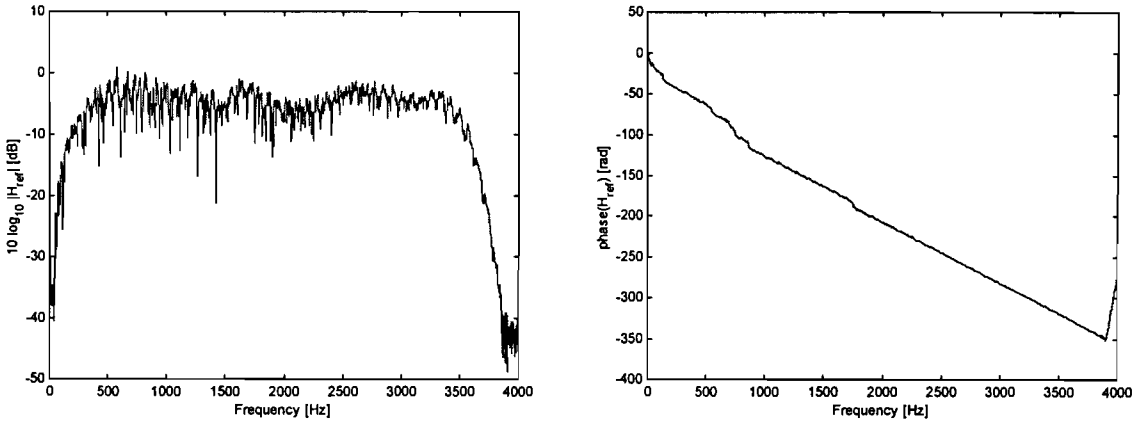

a b

Figure 2.7. Amplitude plot (a) and phase plot (b) of impulse response $\underline{\mathbf{h}}_{ref}$

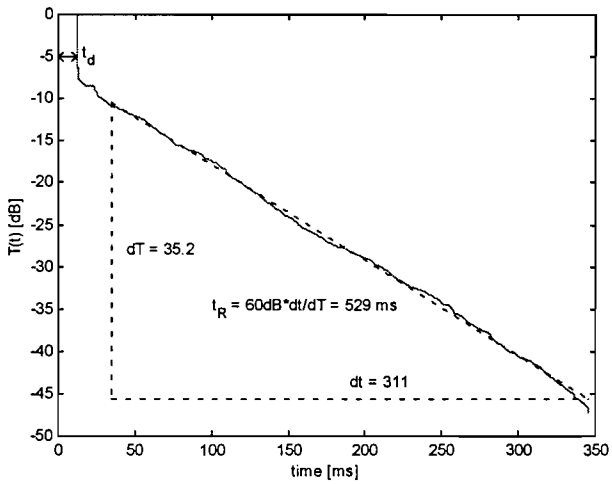

Figure 2.8. Reverberation curve

With this estimated impulse response $\underline{\mathbf{h}}_{ref}$ the reverberation time can be extracted using the reverberation curve, equation (2.19). This reverberation curve is given in figure 2.8. From this curve we can easily distinguish three different parts:

- The flat delay part, this delay is given by $t_d = d_{lm} / c + t_{ADDA}$, with d_{lm} the distance between loudspeaker and microphone and c the velocity of sound and t_{ADDA} represents the delay of the D/A and the A/D converters.
- The direct sound part, this is the steep descent part in the diagram. This is the direct part of the sound power from the loudspeaker that is picked up by the microphone without any reflection. This depends on the position of the loudspeaker and the microphone.
- The diffuse sound part, this is the part with a constant slope. This sound part reaches the microphone with one or more reflection. The slope of the diffuse part determines the reverberation time and depends on the absorption characteristics of the room. In this case the reverberation time t_R = 529 ms.

Measurements with different filter lengths are performed to show the influence of the length of the adaptive filter on the echo-cancellation. For different filter lengths of the adaptive filter the maximal attenuation is measured in dB.

In figure 2.9 the maximal attenuation of the echo-canceller is plotted in the same figure as the reverberation curve. The reverberation curve plots the residual reverberation, or sound power, as a function of time. If the adaptive echo-canceller of a specific duration is used, the residual reverberation can not be cancelled, and thus this residual sound power corresponds to the maximal echo canceling. This means that we can conclude that the maximal attenuation can directly be extracted from the reverberation curve, the longer the duration of the filter, the greater the maximal attenuation. However, the maximum measured attenuation is limited by the background-noise, measured at -43.0 dB.

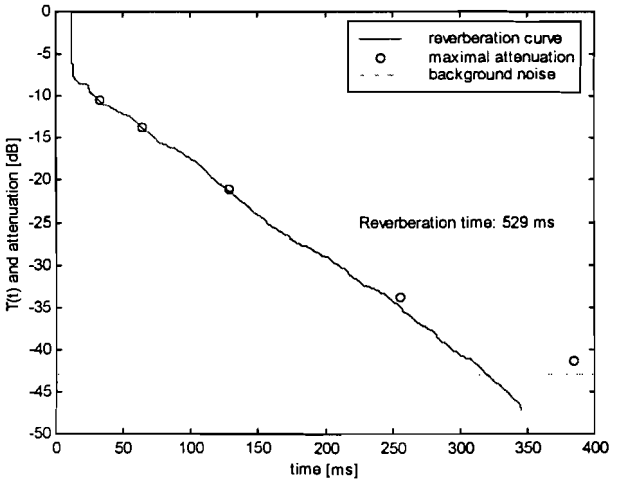

Figure 2.9. Reverberation curve and maximal attenuation as a function of adaptive filter duration

The measurements are repeated using the curtains in the room, the other measurement conditions are equal. The new reverberation curve can be extracted from the identified impulse response.

In figure 2.10 the maximal attenuation of the echo-canceller is plotted in the same figure as the reverberation curve. It is obvious that the slope of the diffuse sound part of the reverberation curve is much steeper in figure 2.10 than in figure 2.9. This means that using these curtains, the reverberation time decreases. It can be concluded that the curtains absorb more sound power than the walls. We can also conclude that the maximal possible attenuation is greater if the reverberation time is shorter, in our case with the curtains. The maximum possible attenuation is again limited by the background-noise, again at –43.0 dB.

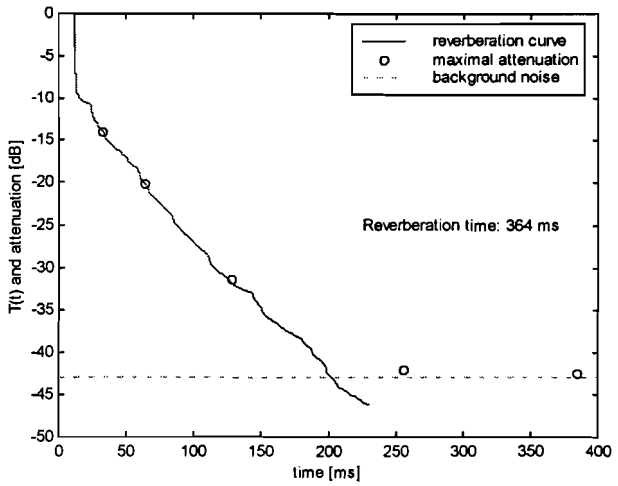

Figure 2.10. Reverberation curve and maximal attenuation as a function of adaptive filter duration, room with curtains

Note that this is only valid if the input signal is white. If the input signal statistics change the maximal attenuation can change [4] and the reverberation curve isn't correct, but can be used as an approximation for the maximal echo-cancellation.

2.3.3. Decorrelation of input signal

In section 2.2 we have introduced the BFDAF. In that section was mentioned was that a correlated input signal decreases the convergence speed of the LMS-algorithm, equation (2.14). Decorrelation of the input signal results in convergence properties independent of the input signal statistics, and therefore enhances the convergence speed. Decorrelation of the input signal is performed in frequency domain using the decorrelated Normalized LMS-algorithm, equation (2.15). In this section a simple example is given that shows the influence of this input signal and the NLMS-algorithm is used to increase convergence speed. Equation (2.16) is used to calculate $\mathbf{P}_x[kL]$.

An auto regressive input signal is used:

$$x[k] = \gamma \cdot x[k-1] + \sqrt{1-\gamma^2} \cdot n[k] \qquad (2.20)$$

With $n[k]$ white noise input signal and γ=0.55.

The power spectrum $\mathbf{P}_x[kL]$ of this auto regressive input signal is not flat (figure 2.11), for low frequencies it has more power and for high frequency it has less power than the flat power spectrum of the white noise signal. Due to this non-flat power spectrum the LMS-algorithm all frequencies will not adapt with the same speed, the higher frequencies will adapt very slow compared to the low frequencies. If we use the Normalized LMS-algorithm the adaptation uses the inverse of the power spectrum $\mathbf{P}_x^{-1}[kL]$ to make the adaptation process independent on the correlation of the input signal.

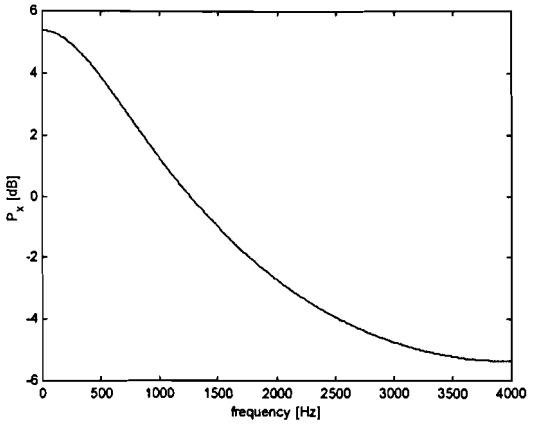

Figure 2.11. Power spectrum of $\mathbf{P}_x$

The difference in convergence speed is significantly, figure 2.12. The LMS-algorithm is slowed down because of the correlated input signal. The decorrelated LMS-algorithm is used to make it independent on the correlation of the input signal.

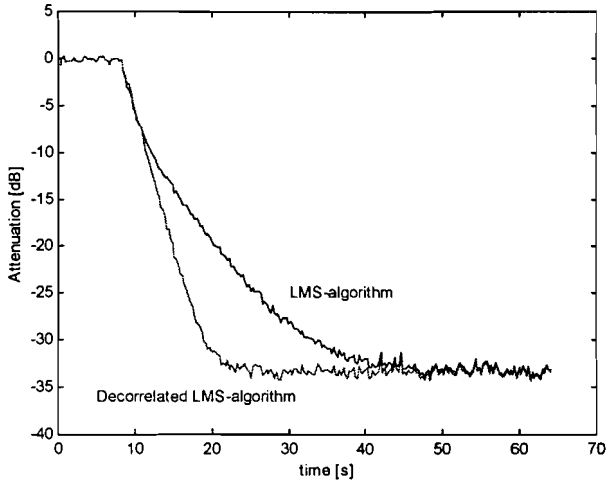

Figure 2.12. Influence of coloured input signal

2.3.4. Influence of unconstrained filtering

In literature [5] unconstrained filtering was already discussed. Not only does it decrease the calculation time by 2 FFT/IFFT's, leaving out operation **G** also increases the maximal attenuation of the echo canceller because it increases the filter length. Negative aspect however is that it produces a wrap-around error. This wrap-around error is not desired.

Only if the adaptive filters are longer than the impulse responses of the system the wrap-around error decreases and the maximal attenuation of the unconstrained filter is equal to the constrained filter. In this case unconstrained filtering is very useful because it decreases the calculation time significantly.

The last $B = 2*L = 4096$ samples of an unconstrained LMS algorithm are saved and plotted in figure 2.13. Notice the large wrap-around error. This is because the adaptive filter $\underline{\mathbf{w}}_M$ is not longer than the impulse response of the acoustical path $\underline{\mathbf{h}}_{ref}$. This wrap-around error is more disturbing than a higher attenuation. Therefore all measurements in this report will be performed using constrained filtering.

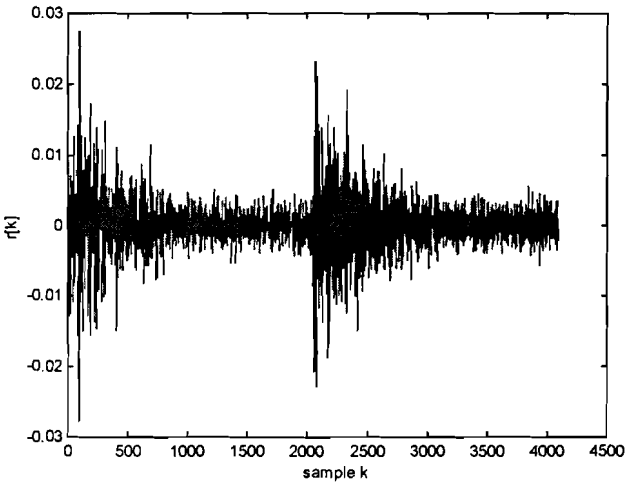

Figure 2.13. Influence of unconstrained BFDAF

2.3.5. Changes of the acoustic path

The acoustic path changes due to movements of microphone or loudspeaker. In this section the position of the microphone is changed in order to observe the resulting effects. The microphone position is changed after 32 seconds. It is moved 2 cm away from the loudspeaker.

Figure 2.14 shows the attenuation of the echo-canceller. If the microphone is moved, the MSE increases and the echo-canceller adapts to the new position. This shows the importance of adaptive filters. If fixed filters are used, the echo-canceller can not adapt to the new position and the MSE remains high.

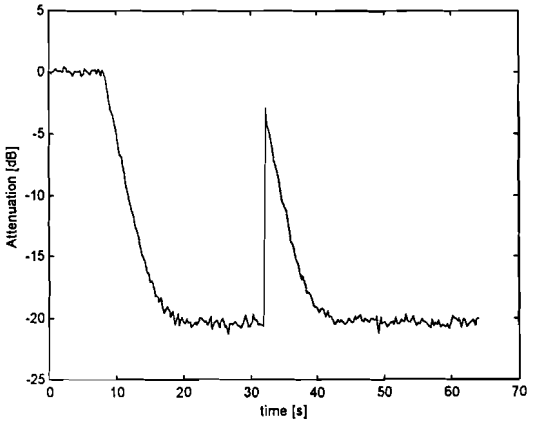

Figure 2.14. Change of the acoustical path

2.4. Conclusions

In this chapter the LMS and the decorrelated LMS algorithm are introduced. An efficient method that uses calculations in frequency domain, BFDAF, is introduced.

The correlation of the input signal decreases the convergence speed of the LMS-algorithm. Decorrelation of the input signal results in an adaptation process independent on the input signal statistics. By measurements it becomes clear that the decorrelated LMS algorithm is very useful if the input signal is correlated.

Room acoustics influence the reverberation and the remaining reverberation limits the maximal attenuation. If the adaptive filter is long, more reverberation can be cancelled, but if it is too short, not all the reverberation can be cancelled and the echo-canceller behaves poor. The reverberation curve can be extracted from the secondary path impulse response. The slope of the reverberation curve determines the reverberation time. If the reverberation time is high, much reverberation remains, and the maximal attenuation decreases. The room acoustics thus have a significance effect on the attenuation.

3. The Filtered-X LMS algorithm

In chapter 1 we have seen that the generation of virtual sound sources requires an adaptive ANC to obtain the filters $\underline{\mathbf{w}}_l$ and $\underline{\mathbf{w}}_r$.

In chapter 2 the echo-canceller was discussed and the LMS and the decorrelated LMS algorithm were introduced. The LMS algorithm is an adaptive algorithm and can be used for identification of an unknown transfer function. Because the adaptation process is dependent on the input signal statistics the decorrelated LMS algorithm was used. This algorithm decorrelates the input signal to make the adaptation process of the LMS algorithm independent on the input signal statistics.

The difference between the echo-canceller and the ANC is that the ANC cancels the noise through an acoustical path. Because of this difference we need a modified LMS algorithm, the so-called Filtered-X LMS algorithm, for the noise-canceller. Derivation of this algorithm is described in section 3.2. In section 3.3 an efficient algorithm, based on the BFDAF in section 2.2, is discussed. The different properties of the filtered-X LMS algorithm are discussed using simulations in section 3.4.

Because the described ANC, section 1.2, consists of two sound sources and two cancellation points, this is called a 2-input 2-output (2-2) ANC. As a start we will use the single-input-single-output (1-1) model as will be discussed in section 3.1. In section 3.4.4 it is extended to a 1-2 input-output noise canceller increasing the robustness of the ANC significantly. The 2-2 input-output noise canceller is described in chapter 4.

3.1. 1-1 Input-output acoustic noise canceling model

In this section the 1-1 input-output acoustic noise canceller will be discussed. This noise canceller is given in figure 3.1. Signal $x[k]$ drives the primary source loudspeaker L_p directly and the secondary loudspeaker L_s is driven by $y[k]$ which is obtained by filtering the input signal $x[k]$ with the acoustic noise canceling filter $\underline{\mathbf{w}}_{ANC}$. The acoustic noise canceling filter $\underline{\mathbf{w}}_{ANC}$ can be derived as described below.

Two equations for the contributions in $r[k]$ can be derived easily in frequency-domain from figure 3.1:

$$\mathbf{R}_{lp} = \mathbf{X} \cdot \mathbf{H}_p \tag{3.1}$$

as a function of the primary source L_p, and

$$\underline{\mathbf{R}}_{ls} = \mathbf{X} \cdot \mathbf{H}_s \cdot \underline{\mathbf{W}}_{ANC} \tag{3.2}$$

as a function of the secondary source L_s.

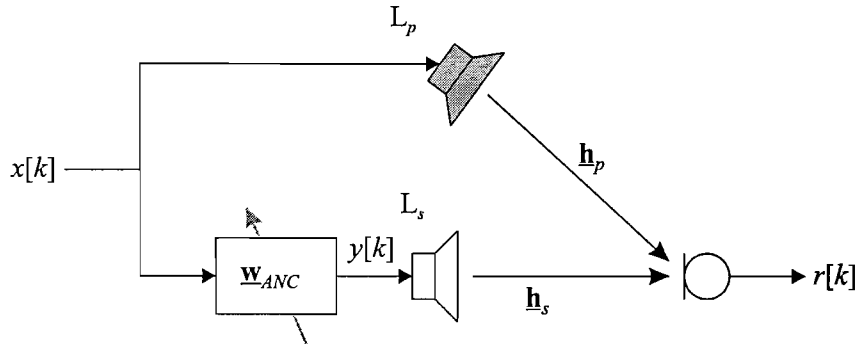

Figure 3.1. Single point acoustic noise cancellation diagram

In the case of acoustic noise canceling, equations (3.2) and (3.1) can be written as:

$$\underline{\mathbf{R}}_{lp} = -\underline{\mathbf{R}}_{ls} \tag{3.3}$$

Combining equations (3.1), (3.2) and (3.3) results in:

$$\underline{\mathbf{H}}_p = -\mathbf{H}_s \cdot \underline{\mathbf{W}}_{ANC} \Rightarrow \underline{\mathbf{W}}_{ANC} = -\mathbf{H}_s^{-1} \cdot \underline{\mathbf{H}}_p \tag{3.4}$$

See also equation (1.12).

This means that both transfer functions, $\underline{\mathbf{H}}_p$ and $\mathbf{H}_s$, need to be identified to calculate $\underline{\mathbf{W}}_{ANC}$. If the filter $\underline{\mathbf{W}}_{ANC}$ is calculated directly from the identified transfer functions this can cause problems:

- Because both transfer functions will change in time due to changes of the position of the sound sources or cancellation point, both transfer functions need to be identified for every new position.
- In general the transfer function $\mathbf{H}_s$ has a non-minimum-phase response, direct inverting will lead to an unstable filter $\underline{\mathbf{W}}_{ANC}$.
- Inverting a zero in $\mathbf{H}_s$ results in a pole in $\underline{\mathbf{W}}_{ANC}$, by this $\underline{\mathbf{W}}_{ANC}$ is an Infinite Impulse Response (IIR) filter. Because the used filter $\underline{\mathbf{W}}_{ANC}$ is a Finite Impulse Response (FIR) filter, this will introduce an error also.

Because of these problems a least squares approach is used to obtain a stable $\underline{\mathbf{W}}_{ANC}$. Adaptive filters will be used to obtain the acoustic noise canceling filters.

3.2. Derivation of the Filtered-X LMS algorithm

In chapter 2 the LMS-algorithm was introduced, using this algorithm it is possible to identify unknown filters. In the situation of an acoustic noise canceller we need to obtain a filter $\underline{\mathbf{W}}_{ANC} = -\mathbf{H}_S^{-1} \cdot \underline{\mathbf{H}}_p$. The main problem obtaining this unknown filter is that this filter is not a physical realizable transfer function and therefore can't be obtained with the normal LMS-algorithm. This means that a modified LMS algorithm has to be used, the so-called Filtered-X LMS algorithm [20].

The Filtered-X LMS algorithm can be derived schematically from the LMS algorithm as shown in figures 3.2a, 3.2b and 3.2c. In figure 3.2a, the normal LMS-algorithm, $\underline{\mathbf{W}}_{ANC}$ has to model the unknown filter $-\mathbf{H}_S^{-1} \cdot \underline{\mathbf{H}}_p$. Problem is that there exists no physical path containing this transfer function, and thus it is not possible to obtain this filter directly using LMS. Therefore, the input signal $\mathbf{X}$ is multiplied by $\mathbf{H}_S$, resulting in figure 3.2b. The unknown filter $\mathbf{H}_S^{-1} \cdot \underline{\mathbf{H}}_p$ is now converted to $\underline{\mathbf{H}}_p$, this

transfer function is physically available. If we assume that the adaptation process takes place on a relatively low time scale, the system is approximately time invariant and linear. This means that the secondary path can be placed behind filter $\underline{\mathbf{W}}_{ANC}$, resulting in figure 3.2c. This is a model of the 1-1 input-output ANC of figure 3.1 and is known as the Filtered-X algorithm. In the update path signal $\mathbf{X}$ is filtered by $\hat{\mathbf{H}}_s$ before updating the filter $\underline{\mathbf{W}}_{ANC}$ in which $\hat{\mathbf{H}}_s$ is an estimate of the real transfer function $\mathbf{H}_s$ and has to be available before adaptation is possible. The necessary accuracy of this estimation will be discussed in section 3.2.1.

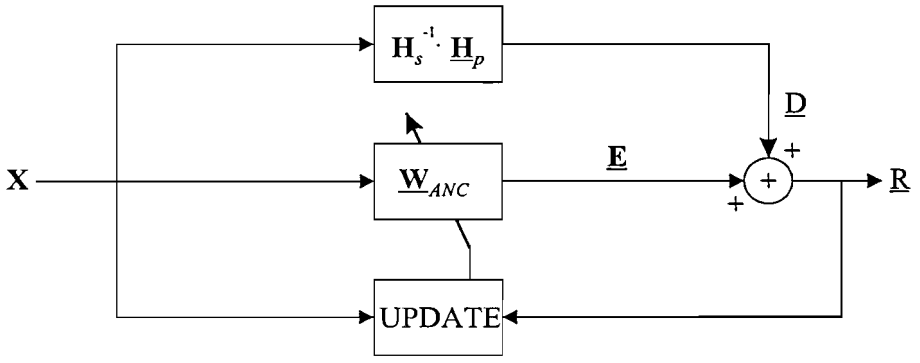

Figure 3.2a. LMS-algorithm to obtain $\underline{\mathbf{W}}_{ANC}$

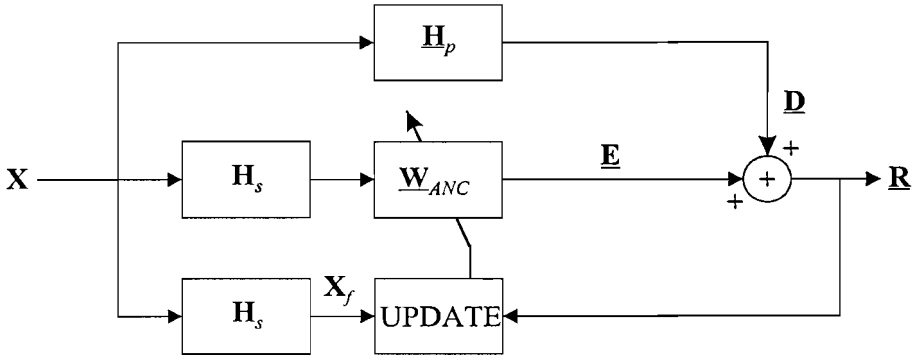

Figure 3.2b. Modified LMS-algorithm

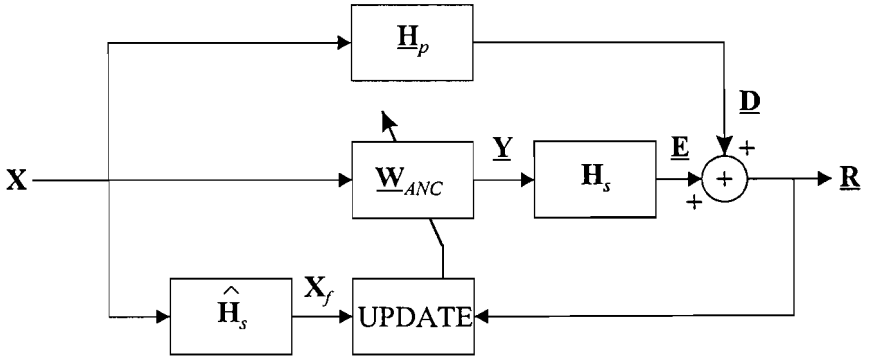

Figure 3.2c. Filtered-X algorithm

The derivation of the Filtered-X LMS algorithm can also start from figure 3.1, the error-signal $r[k]$ can be written in frequency domain as:

$$\mathbf{R} = \mathbf{X} \cdot \mathbf{H}_p + \mathbf{X} \cdot \mathbf{H}_s \cdot \underline{\mathbf{W}}_{ANC} \tag{3.5}$$

It is desired to minimize the mean squared error $E\{\underline{\mathbf{R}}^t \cdot \underline{\mathbf{R}}\}$, in this minimum the gradient of $E\{\underline{\mathbf{R}}^t \cdot \underline{\mathbf{R}}\}$ with respect to $\underline{\mathbf{W}}_{ANC}$ is zero:

$$\min E\{\underline{\mathbf{R}}^t \cdot \underline{\mathbf{R}}\} \Rightarrow \frac{\partial E\{\underline{\mathbf{R}}^t \cdot \underline{\mathbf{R}}\}}{\partial \underline{\mathbf{W}}_{ANC}} = 2 \cdot E\left\{\underline{\mathbf{R}}^t \cdot \frac{\partial \underline{\mathbf{R}}}{\partial \underline{\mathbf{W}}_{ANC}}\right\} = 2 \cdot E\{\mathbf{X} \cdot \mathbf{H}_s \cdot \underline{\mathbf{R}}\} = \underline{0} \tag{3.6}$$

The adaptation algorithm uses this gradient in the update equation to minimize $E\{\underline{\mathbf{R}}^t \cdot \underline{\mathbf{R}}\}$ according to:

$$\underline{\mathbf{W}}_{ANC}[k+1] = \underline{\mathbf{W}}_{ANC}[k] - \alpha \cdot \frac{\partial E\{\underline{\mathbf{R}}^t[k] \cdot \underline{\mathbf{R}}[k]\}}{\partial \underline{\mathbf{W}}_{ANC}[k]} = \underline{\mathbf{W}}_{ANC}[k] - 2 \cdot \alpha \cdot E\{\mathbf{X}[k] \cdot \mathbf{H}_s[k] \cdot \underline{\mathbf{R}}[k]\} \tag{3.7}$$

Because the exact expectation $E\{\mathbf{X}[k] \cdot \mathbf{H}_s[k] \cdot \underline{\mathbf{R}}[k]\}$ is not available an instantaneous estimate of the gradient is used. For the secondary path $\mathbf{H}_s[k]$ we will use an estimate $\hat{\mathbf{H}}_s[k]$ that is identified before filtered-x algorithm is started. This leads to:

$$\underline{\mathbf{W}}_{ANC}[k+1] = \underline{\mathbf{W}}_{ANC}[k] - 2 \cdot \alpha \cdot \mathbf{X}[k] \cdot \hat{\mathbf{H}}_s[k] \cdot \underline{\mathbf{R}}[k]. \tag{3.8}$$

With α the adaptation constant. As already discussed in section 2.1 this adaptation is directly dependent on the correlation of the input $\mathbf{X}$. Correlation of the input leads to a decrease of the convergence speed. Decorrelation leads to an adaptation independent of the input signal's power spectrum $\mathbf{P}_x$. The decorrelated filtered-X LMS-algorithm is

$$\underline{\mathbf{W}}_{ANC}[k+1] = \underline{\mathbf{W}}_{ANC}[k] - 2 \cdot \alpha \cdot \mathbf{P}_x^{-1}[k] \cdot \mathbf{X}[k] \cdot \hat{\mathbf{H}}_s[k] \cdot \underline{\mathbf{R}}[k] \tag{3.9}$$

In the case of filtered-X LMS the adaptation is not only degraded by the input signal but also by the estimate $\hat{\mathbf{H}}_s[k]$, [11, 21]. Normalizing this estimate leads to an all-pass section:

$$\hat{\mathbf{H}}_s[k] / \left|\hat{\mathbf{H}}_s[k]\right| = \arg\left(\hat{\mathbf{H}}_s[k]\right) \tag{3.10}$$

Using this all-pass section leads to:

$$\underline{\mathbf{W}}_{ANC}[k+1] = \underline{\mathbf{W}}_{ANC}[k] - 2 \cdot \alpha \cdot \mathbf{X}[k] \cdot \arg\left(\hat{\mathbf{H}}_s[k]\right) \cdot \underline{\mathbf{R}}[k] \tag{3.11}$$

the use of this all-pass section is already discussed in [1, 2]. It is also possible to combine the normalization and the All-Pass section:

$$\underline{\mathbf{W}}_{ANC}[k+1] = \underline{\mathbf{W}}_{ANC}[k] - 2 \cdot \alpha \cdot \mathbf{P}_x^{-1}[k] \cdot \mathbf{X}[k] \cdot \arg\left(\hat{\mathbf{H}}_s[k]\right) \cdot \underline{\mathbf{R}}[k] \tag{3.12}$$

Simulations will show the effects of this decorrelation and the use of the All-Pass section in section 3.4.

3.2.1. Effect of estimation errors on the Filtered-X LMS algorithm

An estimate of the secondary path is necessary in the update-algorithm of the filtered-X LMS algorithm. The accuracy of that estimation is discussed in literature [10, 12 and 16]. A short description is given here. The estimate of the secondary path impulse response $\underline{\hat{\mathbf{h}}}_s$ can be transformed to frequency samples $\underline{\hat{\mathbf{H}}}_{s,B} = \left(\hat{H}_{s,0}, \hat{H}_{s,2}, .., \hat{H}_{s,B-1}\right)$ using the $(B \times B)$ Fourier matrix $\mathbf{F}_B$.

For every frequency-bin $\hat{H}_{s,i}$ the real secondary path transfer function can be written as:

$$\hat{H}_{s,i} = \left|\hat{H}_{s,i}\right| \cdot \arg\left(\hat{H}_{s,i}\right) \tag{3.13}$$

Errors in the estimation of the secondary path transfer function can be divided in two components:

1. Magnitude errors

From literature it is well known that magnitude errors are not so important. If the All-Pass filtered-X LMS algorithm is used, equation (3.10) and (3.11), the magnitude $|\hat{H}_{s,i}|$ is not even used.

2. Phase errors

Phase errors are more important. From literature it is well known that the filtered-X LMS-algorithm is stable only if the phase-error of the estimation is within 90 degrees for every frequency-bin. The phase error can be written as:

$$\varphi_{e,i} = \left|\arg(H_{s,i}) - \arg(\hat{H}_{s,i})\right| \qquad (3.14)$$

The phase error increases the convergence speed for a specific frequency-bin by an approximate factor $1/\cos(\varphi_{e,i})$ [16].

3.3. Efficient Filtered-X BFDAF

In section 2.2 we have introduced the Block Frequency Domain Adaptive Filter because correlation and convolution operations are calculated in frequency domain more efficient than in time domain. It is possible to extend the BFDAF to a Filtered-X BFDAF, used for the acoustic noise canceller. Two differences are the filtered-X box in the update path and the secondary path $\underline{\mathbf{h}}_s$, see figure 3.3. The filtered-X box is in figure 3.4.

Note that the filtered-X block increases the total number of FFT/IFFT's by 3 to a total of 8. However if the secondary path is fixed, the estimate $\underline{\hat{\mathbf{H}}}_s$ has to be calculated only once, and the total number of FFT/IFFT's is then 7.

The filtered-X box calculates the correct frequency samples $\underline{\mathbf{X}}_{f,B}[kL]$. The correct time samples are calculated using the overlap-save method [15]. This method uses a vector of B input samples $\underline{\mathbf{x}}_B[kL]$ and a filter $\underline{\hat{\mathbf{h}}}_{s,M}[kL]$ of length M. With $B=L+M-1$, this method produces L correct samples $\underline{\mathbf{x}}_{f,L}[kL]$. The correct samples are used in the overlap method to calculated the B frequency samples $\underline{\mathbf{X}}_{f,B}[kL]$ using the DFT.

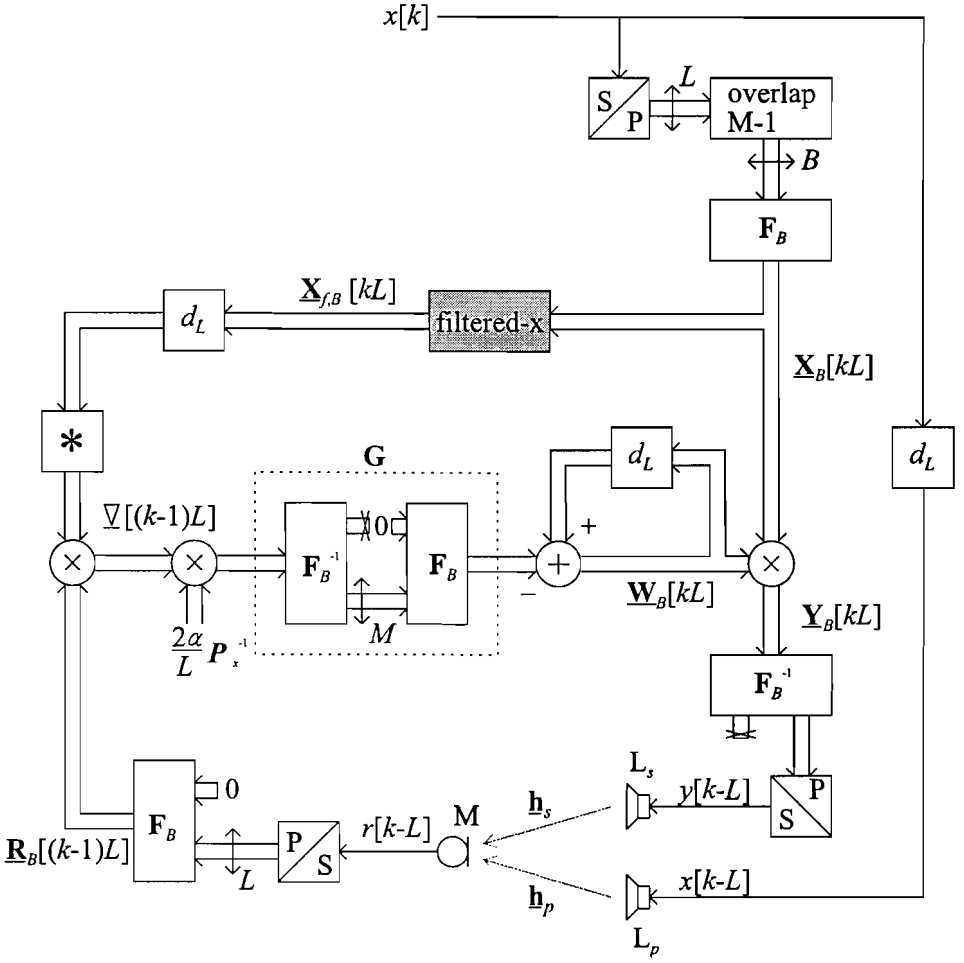

Figure 3.3. Filtered-X Block Frequency Domain Adaptive Filter

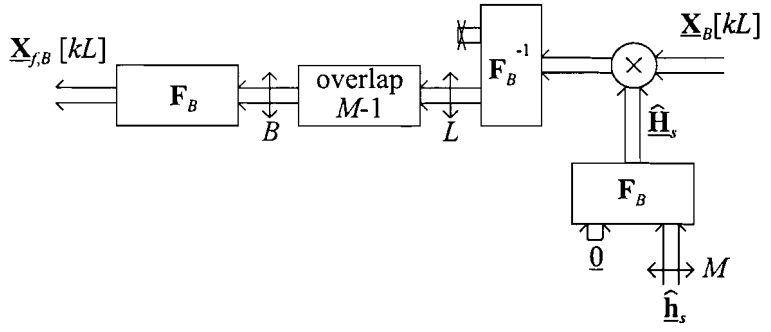

Figure 3.4. Filtered-X box

3.4. Measurements and simulations

In section 2.3 some important properties of the echo canceller were discussed, the correlation of the input signal and the reverberation in the room. In this section will become clear that for the acoustic

noise canceller the secondary path is also very important. Simulations are used to demonstrate the different aspects of the filtered-X LMS algorithm. Before these simulations are possible the primary and the secondary path, $\underline{\mathbf{h}}_p$ and $\underline{\mathbf{h}}_s$, are identified once, using the LMS algorithm of chapter 2, and used in all simulations in this section.

In section 3.2 (with equation (3.9)) was shown that the convergence speed of the filtered-X LMS algorithm not only depends on the correlation of the input-signal but also on the secondary path characteristics. This can easily be described in frequency domain. From literature [11] it is known that at a frequency where the power is relatively low, the convergence speed decreases and it leads to a larger computation error and thus decreases the attenuation. The convergence speed can be improved by using an all-pass section of $\hat{\underline{\mathbf{H}}}_s$, equation (3.11) literature [1, 2]. Simulations of the All-Pass filtered-X LMS algorithm will be discussed in section 3.4.1.

In section 3.4.2 will be discussed that the maximal possible noise cancellation is less dependent on the reverberation in the room but more on the secondary path characteristics, section 3.4.3. The influence of an additional secondary path is given in section 3.4.4. In section 3.4.5 the influence of an estimation error is demonstrated.

In these subsections we will use simulations to show the different properties, but as a start the agreement between measurements and simulations is shown. First, measurements are performed to identify the primary and the secondary path in the room with and without curtains, using the following setup:

- The sampling frequency is 8 kHz.
- The distance between secondary source and microphone is 100 cm.
- The distance between primary source and microphone is 150 cm.
- The blocklength B=4096, the number of new samples L=2048 and thus the filter length is A=2049.

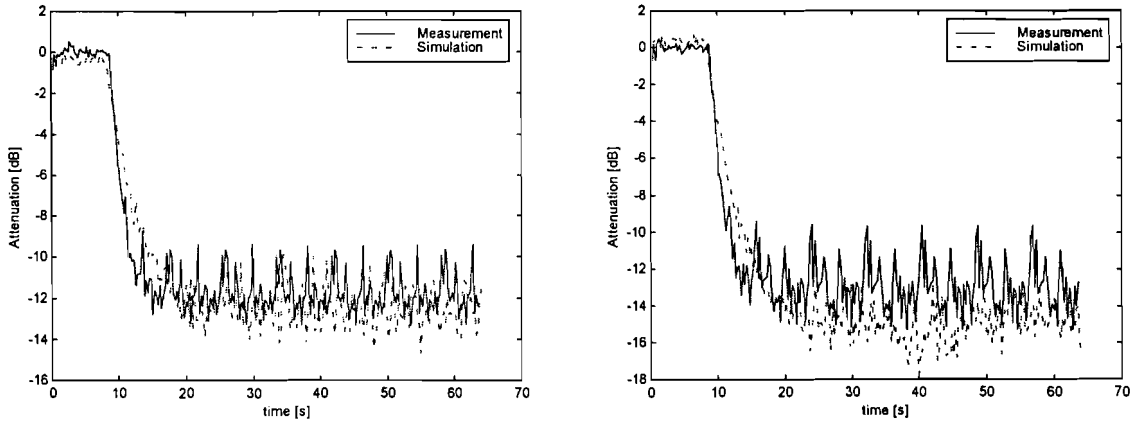

Figure 3.5. Measurement and simulation in room without (a) and with (b) curtains

The estimate of the secondary path is used in the measurement of the noise canceller. The secondary and the primary path are used in a simulation. Curtains are used to show the influence of the reverberation on the acoustic noise canceller. The measurements and the simulations both attenuate the noise equally, see figure 3.5 (a) and (b). Note that the noise canceller attenuates more if the reverberation time is shorter.

In the subsections the identified transfer functions, $\underline{\mathbf{h}}_s$ and $\underline{\mathbf{h}}_p$, are used to demonstrate the different properties of the ANC and the filtered-X LMS algorithm.

3.4.1. Normalization and decorrelation properties

In this section the importance of the normalization and decorrelation is discussed and showed with simulations. There are two different algorithms, as seen in section 3.2:

1. Normalization of the estimate of the secondary path function $\hat{\mathbf{H}}_s$, resulting in the All-pass Filtered-X LMS algorithm
2. Decorrelation of the input signal **X**, resulting in the decorrelated Filtered-X LMS algorithm

First both transfer functions, $\underline{\mathbf{h}}_p$ and $\underline{\mathbf{h}}_s$, are identified using the LMS-algorithm. With these identified transfer functions simulations are used to demonstrate all effects.

Two simulations are performed to demonstrate the influence of the secondary path. First the filtered-X LMS algorithm, equation (3.8), and second the All-Pass filtered-X algorithm, equation (3.11). The adaptation constant is constant in both simulations. A white noise input signal is used to make the adaptation process independent on the input signal statistics.

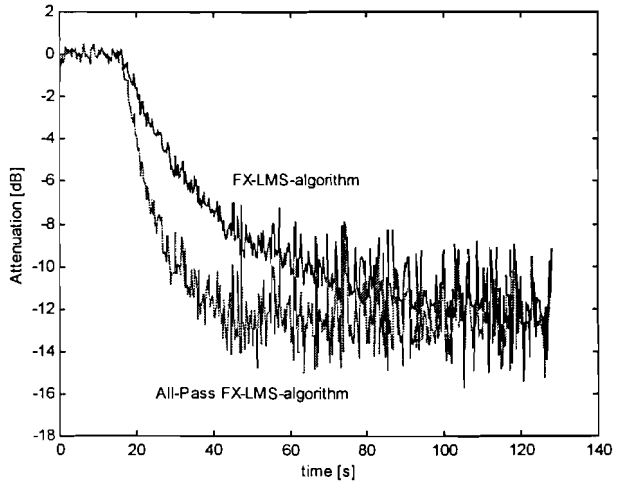

Figure 3.6. Influence of the All-Pass filtered-x LMS algorithm

From figure 3.6 it becomes clear that the secondary path directly influences the speed of convergence. Further on in this report the All-Pass filtered-X LMS algorithm will be used because of its significant advantage compared to the filtered-X LMS algorithm.

To demonstrate the influence of the correlation of the input signal, two different simulations are performed. First the All-Pass filtered-X LMS algorithm and secondly the same algorithm with a decorrelation of the input signal, the All-Pass decorrelated filtered-X LMS algorithm. A correlated input signal is used to demonstrate the effects of this correlated input signal on the convergence speed. The All-Pass estimation of $\mathbf{H}_s$ is used to make the adaptation less dependent on the secondary path transfer function. An auto regressive input signal is used:

$$x[k] = \gamma \cdot x[k-1] + \sqrt{1-\gamma^2} \cdot n[k] \qquad (3.15)$$

With $n[k]$ white noise input signal and γ=0.9. The adaptation constant is constant during the simulations.

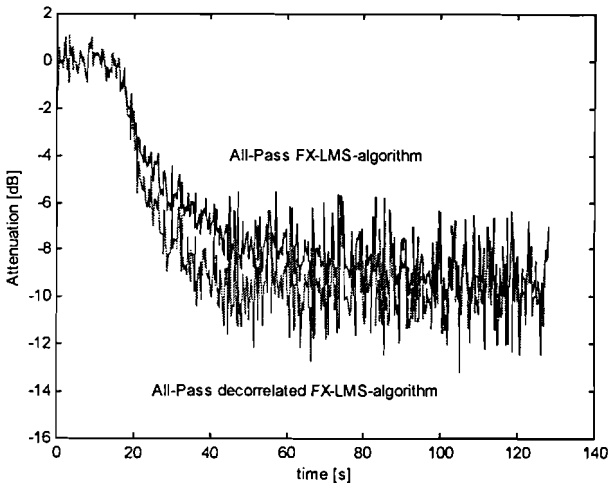

Figure 3.7. Influence of the normalization of the input signal in the All-Pass filtered-x LMS algorithm

From figure 3.7 it becomes clear that the decorrelation of the input signal increases the convergence speed as expected.

Note that the maximal attenuation is not dependent on the All-Pass or the decorrelation method.

3.4.2. Influence of the reverberation on the noise-canceller

In chapter 2 we have discussed that the reverberation time in a room is very important because it determines the maximal echo-cancellation. In this section we will see that the maximal noise-cancellation is not only limited by the reverberation curve but is more dependent on the secondary path characteristics.

In an ideal situation the secondary path can be represented by a pure delay t_{hs}(secondary path frequency response is flat and has a linear phase) coming from the distance from secondary source to microphone and the delay in the A/D and the D/A converters. If this delay is zero the filtered-X LMS algorithm converts to the LMS-algorithm and the maximal noise cancellation can be derived directly from the reverberation curve. If this delay is not zero the delay can be seen as a modeling of the acoustical delay of the identification (LMS-algorithm) of the primary path $\underline{\mathbf{h}}_p$. This modeling virtually extends the adaptive filter by t_{hs}/f_s samples, see also [5]. This means that using this delay the maximal noise-cancellation increases. However, if the delay of the secondary path is greater than the delay of the primary path, $t_{hs} > t_{hp}$, the noise canceling decreases significantly because the first samples can't be identified. The reverberation curve, as derived in chapter 2, changes little: the t_d of the reverberation curve decreases by the delay of the secondary path t_{hs}, resulting in a displacement of the reverberation curve towards the y-axe by t_{hs}.

To show the influence of the reverberation of the room on the noise canceller, curtains are used to decrease the reverberation time in the room, as seen in section 2.3. Both transfer functions, $\underline{\mathbf{h}}_s$ and $\underline{\mathbf{h}}_p$ are identified using the LMS-algorithm for the room without and with the curtains.

First we will use the identified transfer functions of the room without curtains, with a relatively long reverberation time. Simulations with different filter lengths are performed to show the influence of the filter length on the maximal attenuation of the ANC. To make the adaptation process independent on the secondary path characteristics the All-Pass filtered-X LMS algorithm is used to determine the maximal attenuation.

In figure 3.8 the maximal simulated attenuation of the ANC is plotted for different filter lengths in the same figure as the reverberation curve. For short filters the maximal noise cancellation is approximately limited by the reverberation curve, but for long filters the maximal attenuation is degraded by the secondary path characteristics. Increasing the filter length has no effect on the attenuation. From literature [11] and section 3.4.3 it becomes clear that at a frequency-bin where the power is relatively low, this leads to a larger computation error and thus a decrease of attenuation. If the secondary path is a pure delay the reverberation curve determines the maximal attenuation in a noise-cancellation setup.

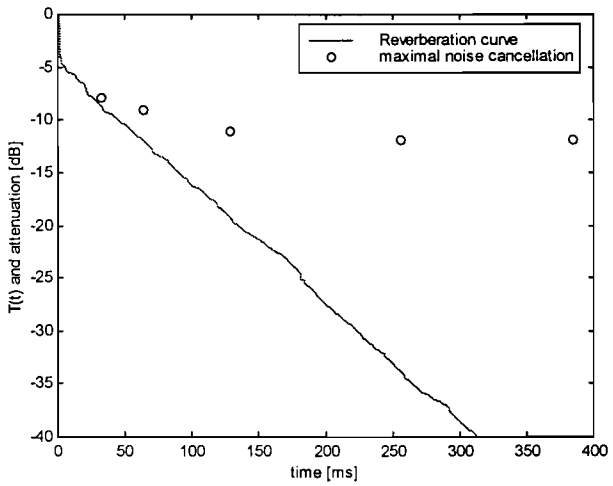

Figure 3.8. Reverberation curve and maximal simulated attenuation as a function of the adaptive filter duration, in the room without curtains

New simulations with a shorter reverberation time are performed, curtains are used to decrease this reverberation time. In figure 3.9, the maximal attenuation of the noise-canceller, for different filter lengths, is plotted in the same figure as the reverberation curve. For short filters the maximal noise cancellation is approximately limited by the reverberation curve again, and for long filters the maximal attenuation is degraded by the secondary path characteristics so that increasing the filter length has no effect on the attenuation.

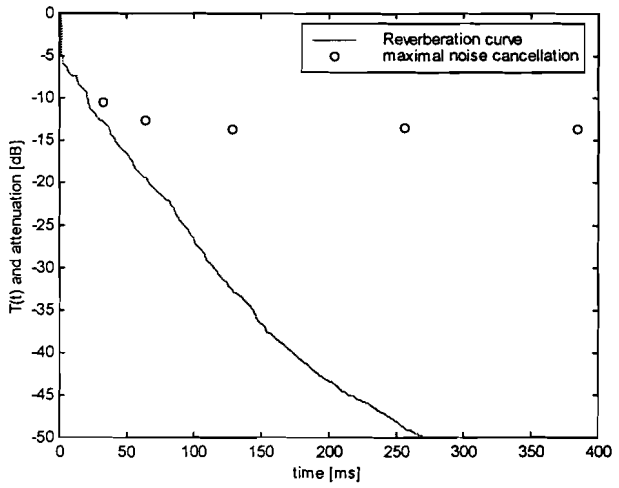

Figure 3.9. Reverberation curve and maximal simulated attenuation as a function of the adaptive filter duration, in the room with curtains

The maximal attenuation with curtains is larger than without curtains, about 2 dB for large filter lengths. The shorter the reverberation time the more the maximal possible attenuation is, but the secondary path characteristics in the room are more important then the reverberation time.

For relatively long filters the maximal attenuation of the acoustic noise canceller is degraded by the secondary path properties, for short filter length the reverberation limits the maximal attenuation.

3.4.3. Influence of the position of the secondary source

In this section the position of the secondary source loudspeaker is changed to alter the secondary path characteristics. The loudspeaker is replaced [6], in the room with curtains, such that the secondary path frequency response contains less frequency-bins where the power is low, because these dips decrease the maximal attenuation, see difference in figure 3.10. The All-pass filtered-X LMS algorithm is used to derive the maximal attenuation. At the new position an increase in attenuation is expected and found with simulations, figure 3.11. Notice that at the frequencies where the power is low the magnitude spectrum of $\underline{\mathbf{R}}$ is high in the steady state condition. The overall attenuation is significantly better at the new position than at the old position.

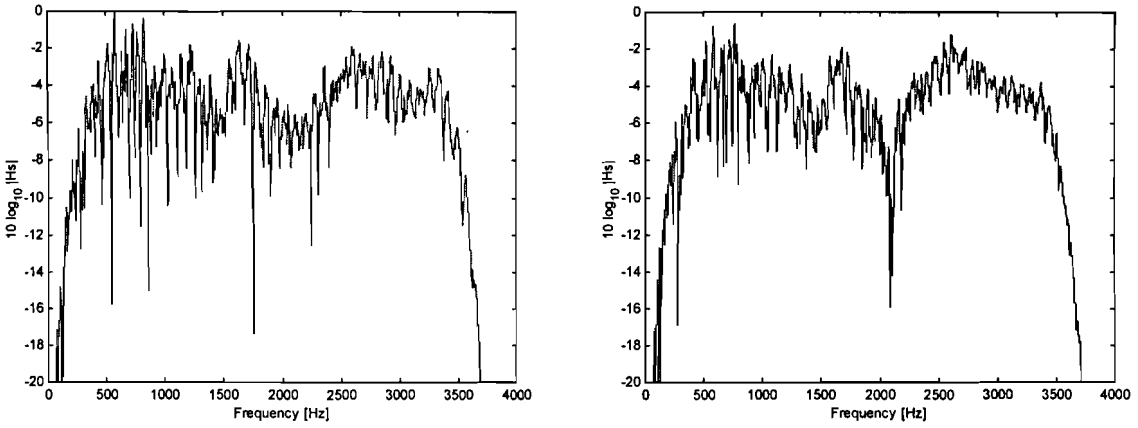

Figure 3.10. Secondary path frequency response, old position (a) and new position (b)

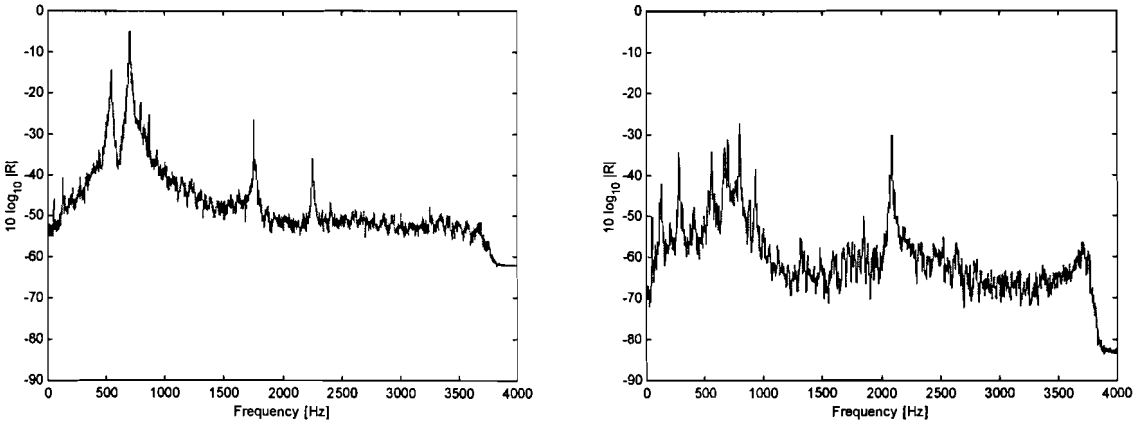

Figure 3.11. Magnitude spectrum of $\underline{\mathbf{R}}$, old position (a) and new position (b)

It is now interesting to show the maximal attenuation for different filter lengths. In figure 3.12 the maximal attenuation of the noise-canceller is plotted for the new position and the old position, the reverberation curve is plotted also. Notice the significant difference in maximal attenuation, for all filter lengths the maximal noise cancellation at the new position is much larger than at the old position. This means that the secondary path characteristics degrade the maximal attenuation.

For large filter lengths the maximal attenuation is lower than the reverberation curve. The reverberation curve can be used as an approximation of the maximal possible noise cancellation.

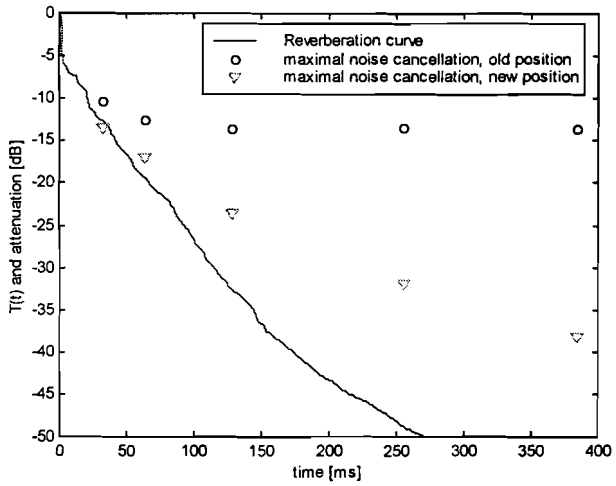

Figure 3.12. Reverberation curve and maximal simulated attenuation as a function of the adaptive filter duration, in the room with curtains

3.4.4. Adding loudspeakers

In this section the 1-1 input-output ANC it is extended to a 1-2 input-output ANC, figure 3.13. Because the secondary path impulse response has non-minimum phases it is impossible to realize exact inverse filtering using the 1-1 input-output ANC, no matter how high the order of the filter is. The exact inverse [14, 18] can be realized using multiple secondary paths, this method is based on MINT (Multiple-input/output INverse Theorem). The exact inverse is possible if both transfer functions do not have common zeros. The results of this theorem will be used.

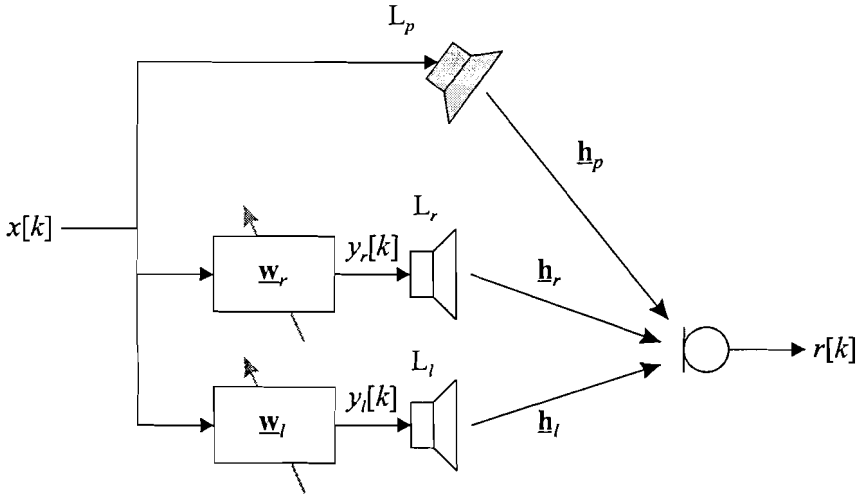

Figure 3.13. The 1-2 input-output noise canceller

This can be evaluated in frequency-domain:

$$\underline{\mathbf{R}} = \mathbf{X} \cdot \underline{\mathbf{H}}_p + \mathbf{X} \cdot \mathbf{H}_r \cdot \underline{\mathbf{W}}_r + \mathbf{X} \cdot \mathbf{H}_l \cdot \underline{\mathbf{W}}_l \qquad (3.16)$$

It is desired that the power of $E\{\underline{\mathbf{R}}' \cdot \underline{\mathbf{R}}\}$ is minimized. Minimizing this function leads to the gradient with respect to $\underline{\mathbf{W}}_r$ and $\underline{\mathbf{W}}_l$:

$$\frac{\partial E\{\underline{\mathbf{R}}^t \cdot \mathbf{R}\}}{\partial \underline{\mathbf{W}}_r} = \underline{\nabla}_r = 2 \cdot E\left\{\underline{\mathbf{R}}^t \cdot \frac{\partial \underline{\mathbf{R}}}{\partial \underline{\mathbf{W}}_r}\right\} = 2 \cdot E\{\mathbf{X} \cdot \mathbf{H}_r \cdot \underline{\mathbf{R}}\} = \underline{0} \quad (3.17)$$

$$\frac{\partial E\{\underline{\mathbf{R}}^t \cdot \mathbf{R}\}}{\partial \underline{\mathbf{W}}_l} = \underline{\nabla}_l = 2 \cdot E\left\{\underline{\mathbf{R}}^t \cdot \frac{\partial \underline{\mathbf{R}}}{\partial \underline{\mathbf{W}}_l}\right\} = 2 \cdot E\{\mathbf{X} \cdot \mathbf{H}_l \cdot \underline{\mathbf{R}}\} = \underline{0} \quad (3.18)$$

The update equations lead to:

$$\underline{\mathbf{W}}_r[k+1] = \underline{\mathbf{W}}_r[k] - \alpha \cdot \underline{\nabla}_r[k] = \underline{\mathbf{W}}_r[k] - 2 \cdot \alpha \cdot E\{\mathbf{X}[k] \cdot \mathbf{H}_r[k] \cdot \underline{\mathbf{R}}[k]\} \quad (3.19)$$

$$\underline{\mathbf{W}}_l[k+1] = \underline{\mathbf{W}}_l[k] - \alpha \cdot \underline{\nabla}_l[k] = \underline{\mathbf{W}}_l[k] - 2 \cdot \alpha \cdot E\{\mathbf{X}[k] \cdot \mathbf{H}_l[k] \cdot \underline{\mathbf{R}}[k]\} \quad (3.20)$$

In section 3.4.1 was showed that the decorrelation of the input signal **X** and the normalization of the secondary path leads to an increase in adaptation speed. This leads to:

$$\underline{\mathbf{W}}_r[k+1] = \underline{\mathbf{W}}_r[k] - 2 \cdot \alpha \cdot \mathbf{P}_x^{-1} \cdot \mathbf{X}[k] \cdot \arg(\hat{\mathbf{H}}_r[k]) \cdot \underline{\mathbf{R}}[k] \quad (3.21)$$

$$\underline{\mathbf{W}}_l[k+1] = \underline{\mathbf{W}}_l[k] - 2 \cdot \alpha \cdot \mathbf{P}_x^{-1} \cdot \mathbf{X}[k] \cdot \arg(\hat{\mathbf{H}}_l[k]) \cdot \underline{\mathbf{R}}[k] \quad (3.22)$$

An instantaneous estimate of the expectations will be used and the secondary paths are estimated before noise canceling.

Simulations are performed to show the influence of the two secondary paths. Figure 3.14 shows the influence of the extra loudspeaker on the noise canceling in the room without curtains. The same measurements are performed in the room with the curtains, figure 3.15. Again it is obvious that the maximal attenuation is better in the room with curtains and thus a shorter reverberation time. Notice that the maximal attenuation is approximately limited by the reverberation curve.

Because inverse filtering is much enhanced using the two secondary paths, the noise canceller performs approximately equivalent to the echo-canceller. This means that only the remaining reverberation limits the maximal attenuation and the secondary path characteristics can be neglected. The reverberation curve can be used as an approximation of the maximal attenuation. Adding more than one extra loudspeaker would have no significance effect on the performance of the ANC for short filter lengths because the remaining reverberation limits the attenuation. However for long filters adding more than one extra loudspeaker would increase the maximal attenuation only little.

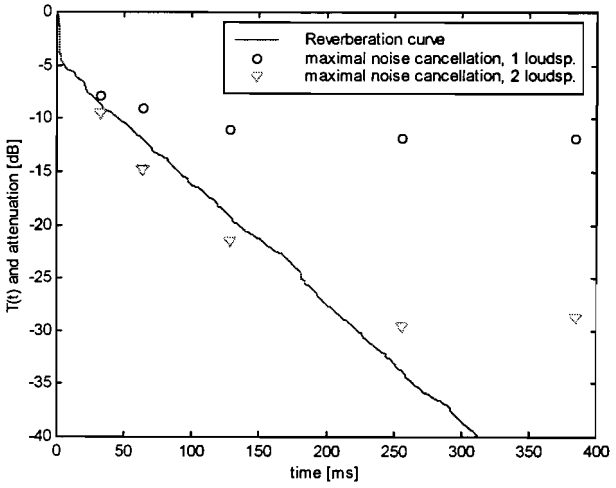

Figure 3.14. Reverberation curve and maximal simulated attenuation as a function of the adaptive filter duration, in the room without curtains

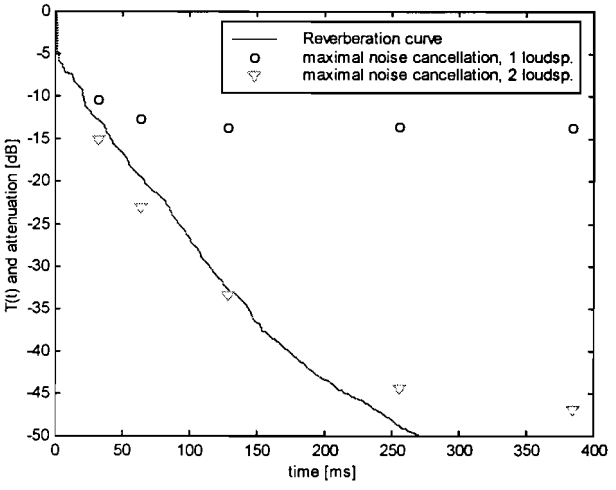

Figure 3.15. Reverberation curve and maximal simulated attenuation as a function of the adaptive filter duration, in the room with curtains

3.4.5. Effect of secondary path estimation errors

The effect of secondary path estimation errors is very important, in section 3.2.1 was already mentioned that the filtered-X LMS-algorithm is stable only if for all frequency samples the phase error is within 90 degrees for all frequency samples.

An estimation error is introduced to demonstrate the influence of this error, investigations are done in [10, 12 and 16]. In this example, for only one frequency sample a phase-error is introduced larger than 90 degrees, this error is 180 degrees. Figure 3.16(a) shows that the attenuation is correct for the first 20 seconds, but after that the error at that specific frequency sample increases and the system becomes unstable. Notice the relatively high error at the specific frequency in figure 3.16(b).

This means that the estimate of the secondary path has to be accurate so that the phase error for all frequencies is smaller than 90 degrees.

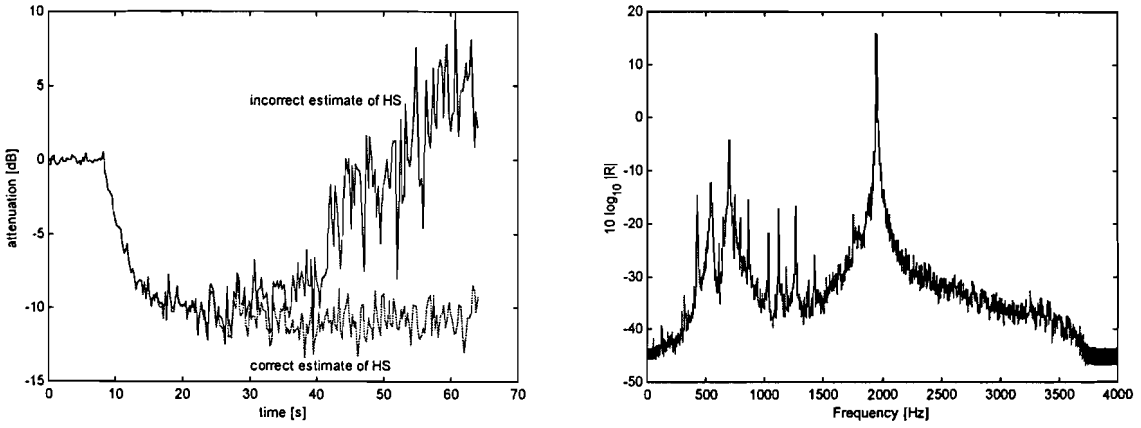

a b

Figure 3.16. Effect of an secondary path estimation error (a) and error spectrum of $\underline{\mathbf{R}}$ (b)

3.5. Conclusions

In this chapter the filtered-X LMS algorithm was introduced. This filtered-X LMS algorithm is used in the acoustic noise canceller. An efficient method, based on BFDAF, is given in section 3.3.

With simulations the different aspects of the filtered-X LMS algorithm become clear. It is discussed that the secondary path influences the maximal noise cancellation such that for frequencies where the power is relatively low, the convergence speed decreases and it leads to a larger computation error and thus a decrease of attenuation. Normalization of the secondary path increases the convergence speed because the system makes the adaptation independent on the secondary path statistics. The correlation of the input signal also degrades the convergence speed, normalization of the input signal increases the adaptation speed because the adaptation is not influenced by the input signal statistics.

The secondary path frequencies where the power is relatively low the maximal attenuation is limited. Changing the position of the secondary source changes the secondary path statistics and can change the maximal attenuation significantly.

In chapter 2 we have seen that the echo canceling can be directly determined from the reverberation curve. This is not true in case of noise canceling. The maximal noise canceling is significantly lower than the maximal echo canceling with the same filter length, this is because the maximal echo canceling is degraded by the secondary path characteristics. For large filter lengths the maximal attenuation is limited by the influence of the secondary path and for short filter length the maximal attenuation can be approximated by the reverberation curve.

If more than one loudspeaker are used, the inverse filtering performs significantly better than if only one loudspeaker is used. This is because the extra secondary paths compensate for those frequencies where the power is low. The maximal attenuation is now approximately equivalent to the echo-canceller and is thus determined by the reverberation curve.

4. Multiple filtered-X LMS algorithm

In chapter 3 it was discussed that the performance of the 2-1 input output ANC behaves much better than the 1-1 input-output ANC. This is because the other secondary acoustic path accounts for the zeros in the secondary path.

In this chapter the 2-2 input-output ANC is discussed [8, 19]. In section 4.1 the derivation of the system is given and in section 4.2 the performance of the 2-2 input-output ANC is discussed using measurements and simulations.

4.1. Derivation of the system

This section will start with recalling figure 1.1 of chapter 1. This figure 4.1 is used to derive the equations for the 2-2 input-output ANC.

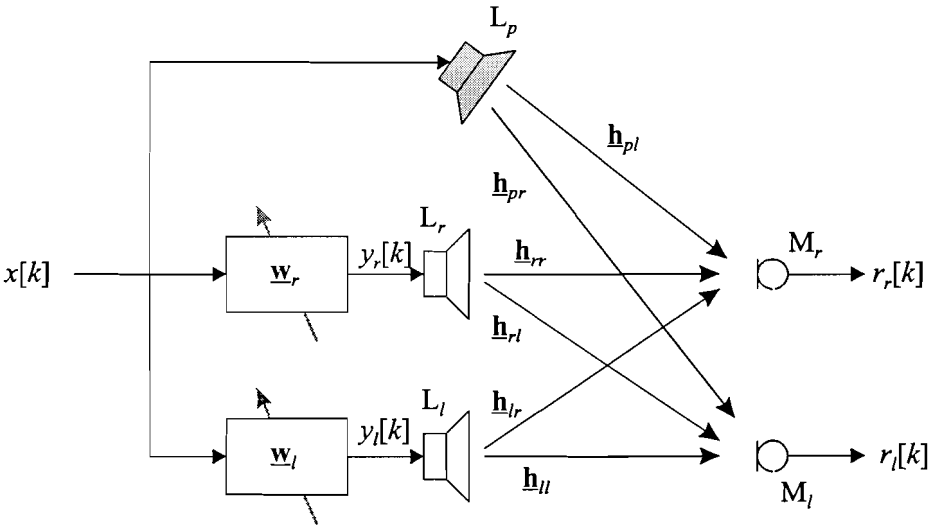

Figure 4.1. 2-2 input-output ANC

For the signal $r_r[k]$ and $r_l[k]$ can be derived in frequency domain:

$$\underline{\mathbf{R}}_r = \mathbf{X}\cdot\underline{\mathbf{H}}_{pr} + \mathbf{X}\cdot\mathbf{H}_{rr}\cdot\underline{\mathbf{W}}_r + \mathbf{X}\cdot\mathbf{H}_{lr}\cdot\underline{\mathbf{W}}_l \qquad (4.1)$$

$$\underline{\mathbf{R}}_l = \mathbf{X}\cdot\underline{\mathbf{H}}_{pl} + \mathbf{X}\cdot\mathbf{H}_{sll}\cdot\underline{\mathbf{W}}_l + \mathbf{X}\cdot\mathbf{H}_{srl}\cdot\underline{\mathbf{W}}_r \qquad (4.2)$$

As an error-criterion we will use:

$$\min\left(E\left\{\underline{\mathbf{R}}_r^t\cdot\underline{\mathbf{R}}_r\right\} + E\left\{\underline{\mathbf{R}}_l^t\cdot\underline{\mathbf{R}}_l\right\}\right) \qquad (4.3)$$

It is desired that this cost function is minimized. Calculating the gradient with respect to $\underline{\mathbf{W}}_r$ and $\underline{\mathbf{W}}_l$ does this. This leads to:

$$\frac{\partial E\{\underline{\mathbf{R}}_r^2\}+E\{\underline{\mathbf{R}}_l^2\}}{\partial \underline{\mathbf{W}}_r}=\underline{\nabla}_r \quad \begin{aligned}&=2\cdot E\left\{\mathbf{R}_r\cdot\frac{\partial \underline{\mathbf{R}}_r}{\partial \underline{\mathbf{W}}_r}\right\}+2\cdot E\left\{\mathbf{R}_l\cdot\frac{\partial \underline{\mathbf{R}}_l}{\partial \underline{\mathbf{W}}_r}\right\}\\&=2\cdot E\{\mathbf{X}\cdot\mathbf{H}_{rr}\cdot\mathbf{R}_r\}+2\cdot E\{\mathbf{X}\cdot\mathbf{H}_{rl}\cdot\mathbf{R}_l\}=\underline{0}\end{aligned} \tag{4.4}$$

$$\frac{\partial E\{\underline{\mathbf{R}}_r^2\}+E\{\underline{\mathbf{R}}_l^2\}}{\partial \underline{\mathbf{W}}_l}=\underline{\nabla}_l \quad \begin{aligned}&=2\cdot E\left\{\mathbf{R}_r\cdot\frac{\partial \underline{\mathbf{R}}_r}{\partial \underline{\mathbf{W}}_l}\right\}+2\cdot E\left\{\mathbf{R}_l\cdot\frac{\partial \underline{\mathbf{R}}_l}{\partial \underline{\mathbf{W}}_l}\right\}\\&=2\cdot E\{\mathbf{X}\cdot\mathbf{H}_{lr}\cdot\mathbf{R}_r\}+2\cdot E\{\mathbf{X}\cdot\mathbf{H}_{ll}\cdot\mathbf{R}_l\}=\underline{0}\end{aligned} \tag{4.5}$$

The update equations lead to:

$$\underline{\mathbf{W}}_r[k+1]=\underline{\mathbf{W}}_r[k]-\alpha\cdot\underline{\nabla}_r[k]\approx\underline{\mathbf{W}}_r[k]-2\cdot\alpha\cdot\{\mathbf{X}[k]\cdot\mathbf{H}_{rr}[k]\cdot\underline{\mathbf{R}}_r[k]+\mathbf{X}[k]\cdot\mathbf{H}_{rl}[k]\cdot\underline{\mathbf{R}}_l[k]\} \tag{4.6}$$

$$\underline{\mathbf{W}}_l[k+1]=\underline{\mathbf{W}}_l[k]-\alpha\cdot\underline{\nabla}_l[k]\approx\underline{\mathbf{W}}_l[k]-2\cdot\alpha\cdot\{\mathbf{X}[k]\cdot\mathbf{H}_{lr}[k]\cdot\underline{\mathbf{R}}_r[k]+\mathbf{X}[k]\cdot\mathbf{H}_{ll}[k]\cdot\underline{\mathbf{R}}_l[k]\} \tag{4.7}$$

In chapter 2 and 3 we discussed that the decorrelation of the input signal **X** and the normalization of the secondary path leads to an increase in adaptation speed. This leads to:

$$\underline{\mathbf{W}}_r[k+1]=\underline{\mathbf{W}}_r[k]-2\cdot\alpha\cdot\mathbf{P}_x^{-1}\cdot\{\mathbf{X}[k]\cdot\arg(\hat{\mathbf{H}}_{rr}[k])\cdot\underline{\mathbf{R}}_r[k]+\mathbf{X}[k]\cdot\arg(\hat{\mathbf{H}}_{rl}[k])\cdot\underline{\mathbf{R}}_l[k]\} \tag{4.8}$$

$$\underline{\mathbf{W}}_l[k+1]=\underline{\mathbf{W}}_l[k]-2\cdot\alpha\cdot\mathbf{P}_x^{-1}\cdot\{\mathbf{X}[k]\cdot\arg(\hat{\mathbf{H}}_{lr}[k])\cdot\underline{\mathbf{R}}_r[k]+\mathbf{X}[k]\cdot\arg(\hat{\mathbf{H}}_{ll}[k])\cdot\underline{\mathbf{R}}_l[k]\} \tag{4.9}$$

Figure 4.2 gives the update algorithm for $\underline{\mathbf{W}}_r$, the update algorithm for $\underline{\mathbf{W}}_l$ is almost equivalent, see equations 4.8 and 4.9.

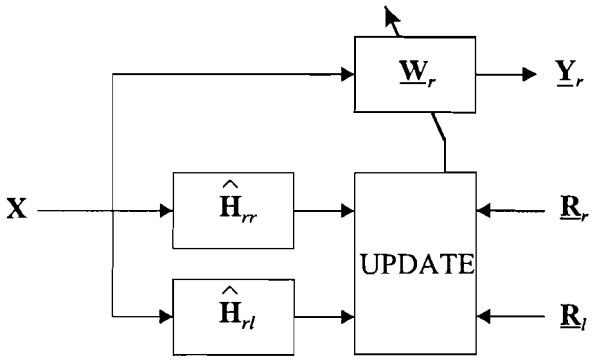

Figure 4.2. Update algorithm for $\underline{\mathbf{W}}_r$

4.2. Measurements and simulations

Measurements are performed to show the agreement between the measurements and the simulations. Before the measurements are possible the secondary paths, $\underline{\mathbf{h}}_{rr}$, $\underline{\mathbf{h}}_{lr}$, $\underline{\mathbf{h}}_{rl}$ and $\underline{\mathbf{h}}_{ll}$, have to be identified using the LMS algorithm of chapter 2. Not only the secondary, but also the primary paths, $\underline{\mathbf{h}}_{pr}$ and $\underline{\mathbf{h}}_{pl}$, are identified because these are used in the simulations. The acoustical paths are identified in the room with and without the curtains.

Two simple measurements are performed to show the maximal attenuation. The measurement setup is as follows:

- The sampling frequency is 8 kHz.
- The positions of primary and secondary sources and microphones are illustrated in figure 4.3.
- The blocklength B=4096, the number of new samples L=2300 and thus the filter length is A=1797.

2300 input samples are necessary because the calculation time of the 2-2 input-output ANC takes about $2300*f_s$ seconds to calculate complete filter.

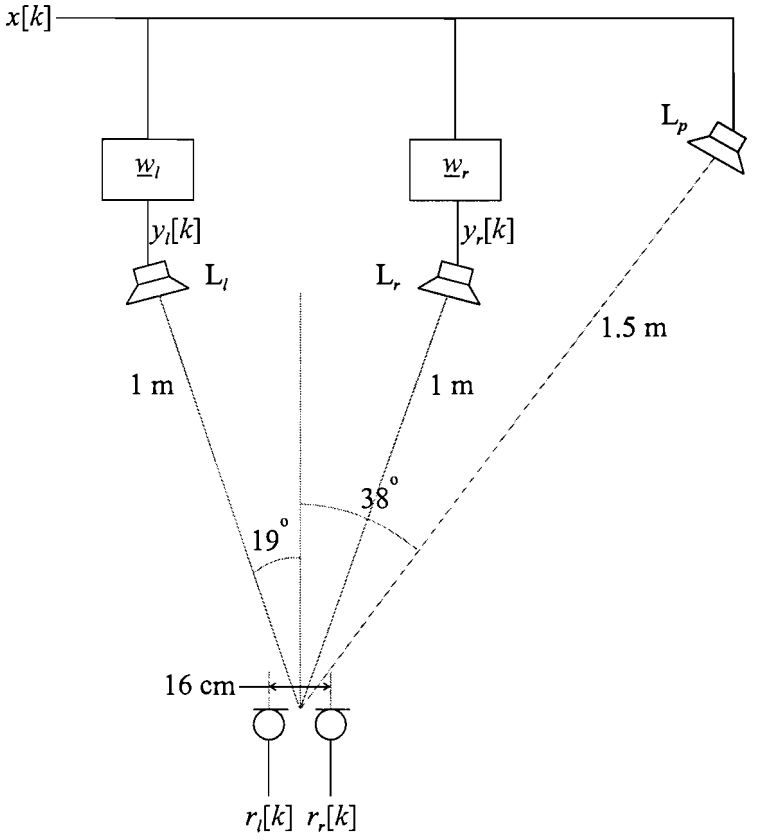

Figure 4.3. Measurement setup

Measurements are performed first in the room without curtains and later in the room with the curtains, using the above-mentioned setup. Both for the left microphone and the right microphone the error signal $r_l[k]$ and $r_r[k]$ are measured. The attenuation is measured as a function of $E\{d_r^2[kL]\}$. $E\{d_r^2[kL]\}$ is $E\{r_r^2[kL]\}$ without noise canceling. This leads to:

$$Att_r = E\{r_r^2[kL]\} / E\{d_r^2[kL]\} \qquad (4.10)$$

$$Att_l = E\{r_l^2[kL]\} / E\{d_r^2[kL]\} \qquad (4.11)$$

The first 8 seconds no adaptation is performed to measure $E\{d_r^2[kL]\}$. In figure 4.4 the error signals are plotted during the measurements in both the room without and with the curtains. In figure 4.5 these measurements are repeated using simulations.

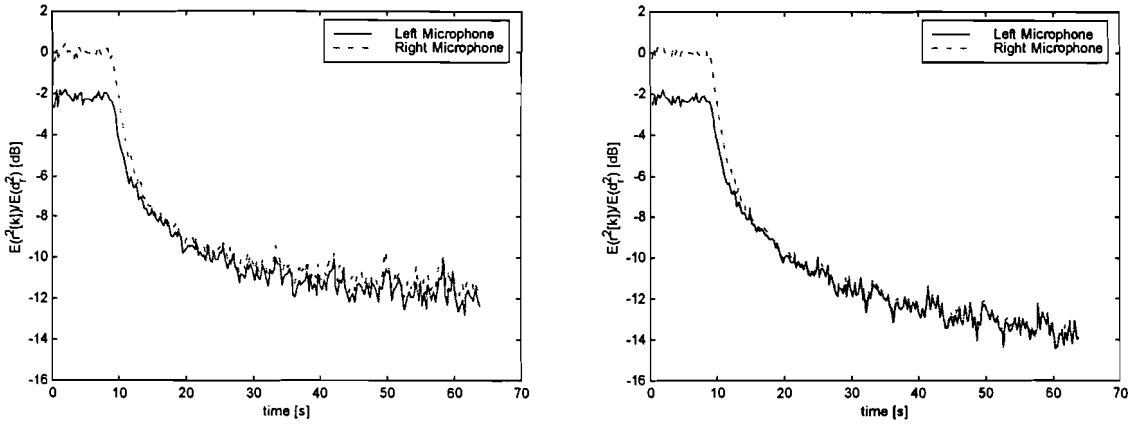

Figure 4.4. Measurements on the 2-2 input-output ANC in room without (a) and with (b) curtains

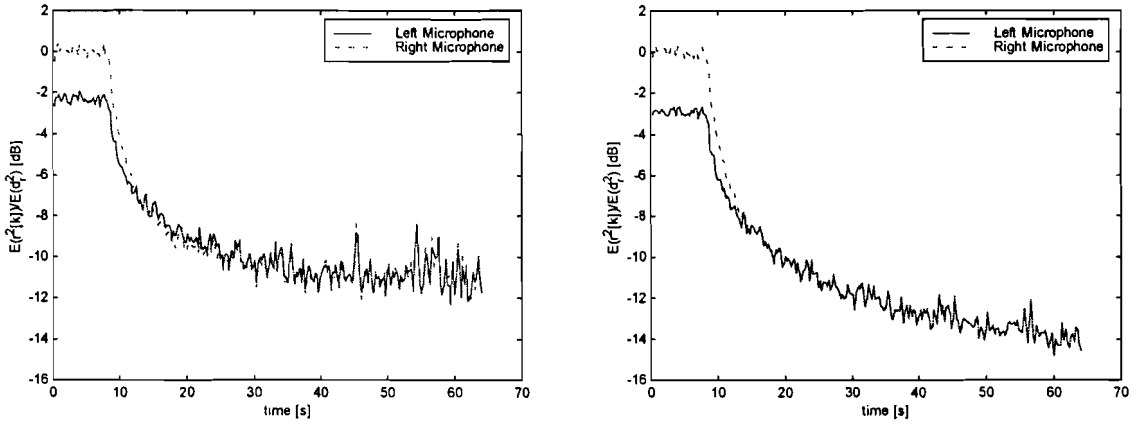

Figure 4.5. Simulations on the 2-2 input-output ANC in room without (a) and with (b) curtains

The right microphone is placed at a shorter distance of the primary loudspeaker, therefore the power $E\{d_l^2[kL]\} < E\{d_r^2[kL]\}$. Note that the adaptation speed and the attenuation in the measurements are similar to the simulations. Using this we can simulate the behavior of different filter lengths (figure 4.6 and 4.7). Not only the 2-2 but also the 1-1 and the 1-2 input-output ANC are plotted in these figure, this is to compare the behavior of the 2-2 input-output ANC with the other ANC's. Simulations are performed in the room without curtains, figure 4.6, and the room with curtains, figure 4.7. In both figures the reverberation curve is also plotted to compare the ANC with the echo-canceller.

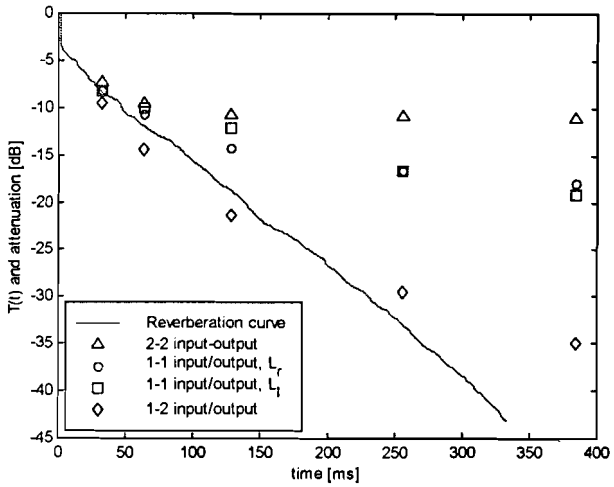

Figure 4.6. Reverberation curve and maximal attenuation as a function of the adaptive filter duration, in the room without curtains

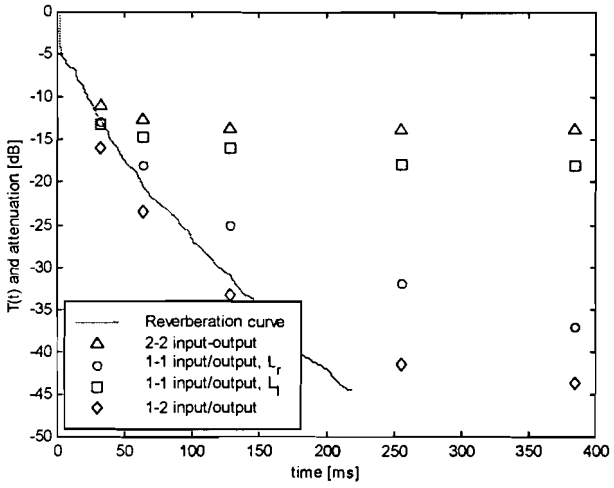

Figure 4.7. Reverberation curve and maximal attenuation as a function of the adaptive filter duration, in the room with curtains

It is very obvious that the performance of the 2-2 input-output ANC behaves worse compared to the 1-1 and the 1-2 input-output ANC. The reverberation curve limits the attenuation for small filter lengths and for large filter lengths the secondary path degrade the performance, this is also stated in chapter 3. In chapter 3 we have also seen that increasing the number of loudspeakers has a significance positive effect on the ANC. If an extra loudspeaker is used it is expected that the performance would increase.

In the room with curtains, the maximal attenuation of the right loudspeaker is much better than the left loudspeaker. This is because the maximal attenuation is dependent on the secondary path characteristics.

Note that the maximal attenuation of the ANC is enhanced if the reverberation time is shorter.

4.3. Conclusions

The 2-2 input-output ANC is used to realize a virtual sound source generator, the behavior of the ANC is significantly worse compared to the 1-1 or the 1-2 input-output ANC. This is because the secondary path characteristics degrade the maximal attenuation. For short filter lengths the attenuation is limited by the remaining reverberation.

5. Online modeling of the secondary paths

In chapter 3 the filtered-X LMS algorithm was introduced and discussed that the filtered-X LMS algorithm requires an accurate estimate of the secondary path to ensure convergence: the phase error of this secondary path estimate has to be within 90 degrees for every frequency-bin. The secondary path characteristics change due to movements of the secondary source or the microphone. If the filtered-X LMS algorithm uses a fixed estimate of the secondary path, these movements will introduce phase errors that can exceed the 90 degrees limitation and the filtered-X LMS algorithm becomes unstable. If these changes of the secondary path can be tracked using online modeling techniques this increases the robustness of the algorithm.

In section 5.1 the effect of changes in the secondary path is illustrated. Current online modeling techniques can be divided into two classes, namely techniques that use additive noise to estimate the secondary path and techniques that don't use this additive noise. These techniques are discussed in section 5.3 and section 5.2 respectively. A new modeling technique that uses an additive noise signal is described in section 5.3.2. The results of this new technique are promising but need to be more researched. In this chapter the 1-1 input-output ANC is discussed for simplicity.

5.1. Effect of changes in the secondary path

The main problem is that changing the position of microphone or secondary sources changes the secondary path. If the estimate of $\mathbf{H}_s$ is fixed, these changes in the secondary path can lead to phase errors larger then 90 degrees and the filtered-X method becomes unstable. To illustrate the effect of movements of the microphone the secondary path is identified at 5 different microphone positions, see figure 5.1.

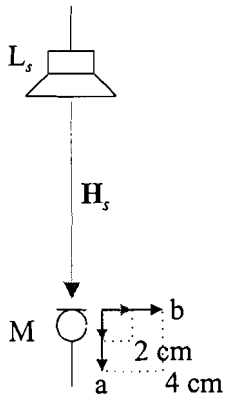

Figure 5.1. Secondary path measured at 5 different positions

First the microphone is replaced at a position 2 cm and 4 cm from the original position in the line of secondary source L_s to microphone, movement 'a' in figure 5.1. To demonstrate the effects of these movements the phase errors are plotted in figure 5.2a respectively 5.2b. The phase error is approximately linear with the frequency and with the displacement of the microphone.

Note that for low frequencies (<200 Hz) and for high frequencies (>3800 Hz) the phase is disturbed by the attenuation properties of microphone amplifier and the A/D and D/A converters respectively. Therefore we are only interested in the phase error for frequencies between the 200 and 3800 Hz.

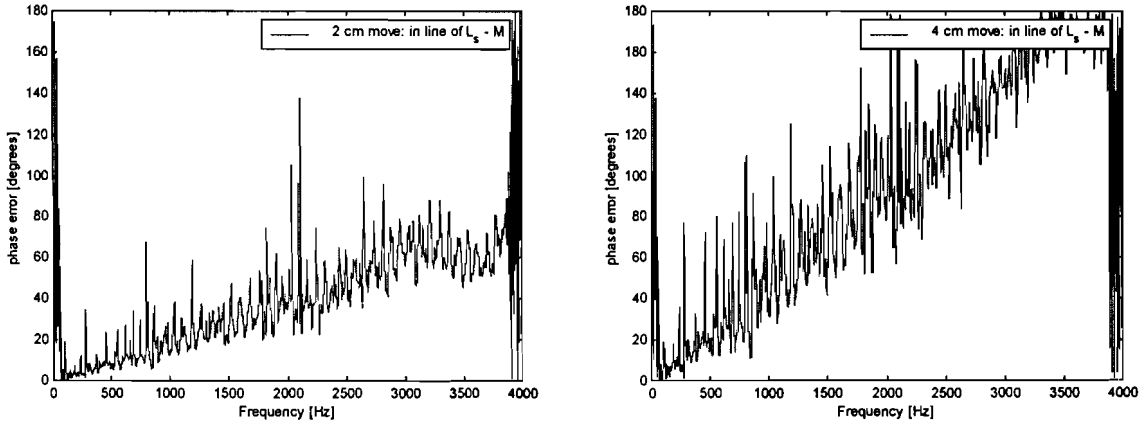

Figure 5.2. Phase error as a function of a movements in the line of loudspeaker and microphone, 2 cm (a) and 4 cm (b)

Figure 5.3 shows the error phase as a result of a displacement adjacent to the line from loudspeaker to microphone, movement 'b' in figure 5.1. In this case the distances from secondary source to microphone are almost equal. Figure 5.3a shows a displacement of 2 cm and figure 5.3b a displacement of 4 cm. In both cases the phase error is not large, the phase error is higher than 90 degrees for only 1 frequency-bin.

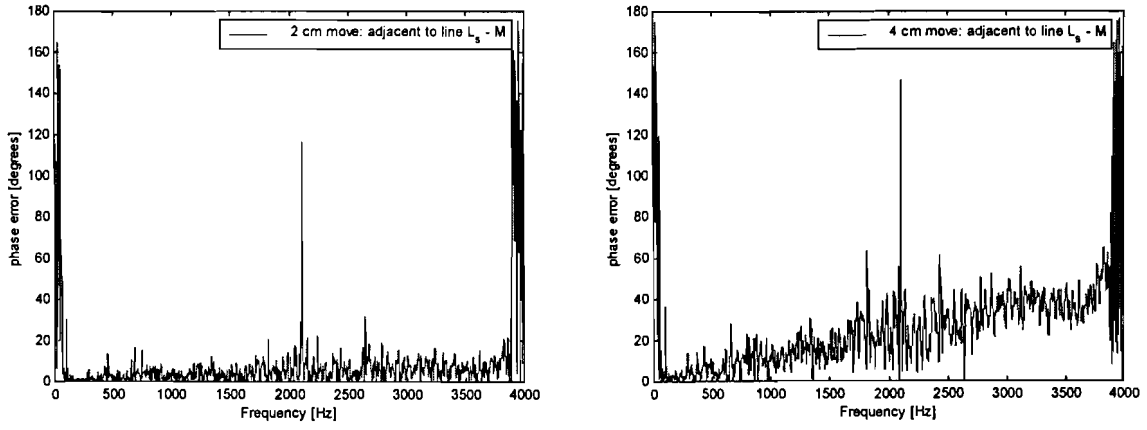

Figure 5.3. Phase error as a function of a movements adjacent to the line of loudspeaker to microphone, 2 cm (a) and 4 cm (b)

This means that moving the microphone away or closer to the loudspeaker leads to a phase error linear with this displacement and linear with frequency. If the microphone is moved and the distance from microphone to loudspeaker is equal, the phase error is significantly smaller. Stable filtered-X is only possible for small movements and if the distance between secondary source and the microphone is approximately constant.

Changing the position of the microphone or the loudspeaker changes the secondary path and for these errors the system has to account for, this is done with online modeling. In the next sections online modeling techniques of the secondary path are described and the properties of these techniques are discussed.

5.2. Online modeling of the secondary path

In the previous section is discussed that online modeling of the secondary path is necessary if the secondary path changes. In this section 3 methods are discussed to model the secondary path online. The advantage of these algorithms is that they use no extra training signal to model the secondary path.

5.2.1. Online modeling of the delay of the secondary path

A relatively simple algorithm is the online estimation of the delay of the secondary path. Because only a pure delay is used as estimate for the secondary path the filtered-X LMS algorithm is called the delayed-X LMS algorithm [3]. The use of this algorithm is only possible if the phase error not exceeds the 90 degrees limitation for stable filtered-X.

The phase error between the measured transfer function and the pure delay is calculated. The optimal delay of the system is approximately 95-96 samples. Figure 5.4a and 5.4b show the phase error if the secondary path is estimated by a pure delay of 95 respectively 96 samples. For many frequency-bins the phase error exceeds the 90 degrees limitation. The delayed-X LMS algorithm will be unstable in this situation and a method that tracks the delay of the system is not useful here.

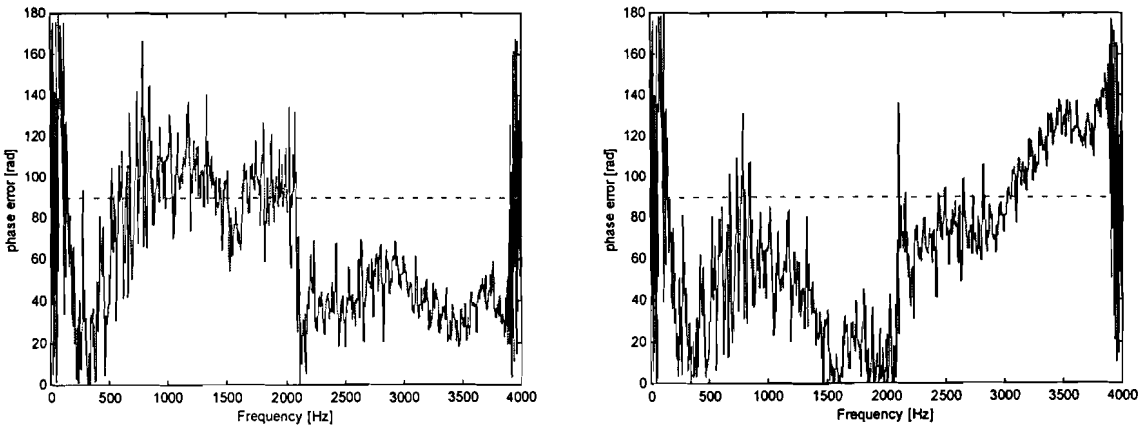

a b

Figure 5.4. Phase error with a delay of 95 (a) and 96 (b) samples

5.2.2. Online modeling parallel to the secondary path

A simple method of online modeling is an identification algorithm directly parallel on the secondary path, see figure 5.5. An extra LMS method is used to model this path.

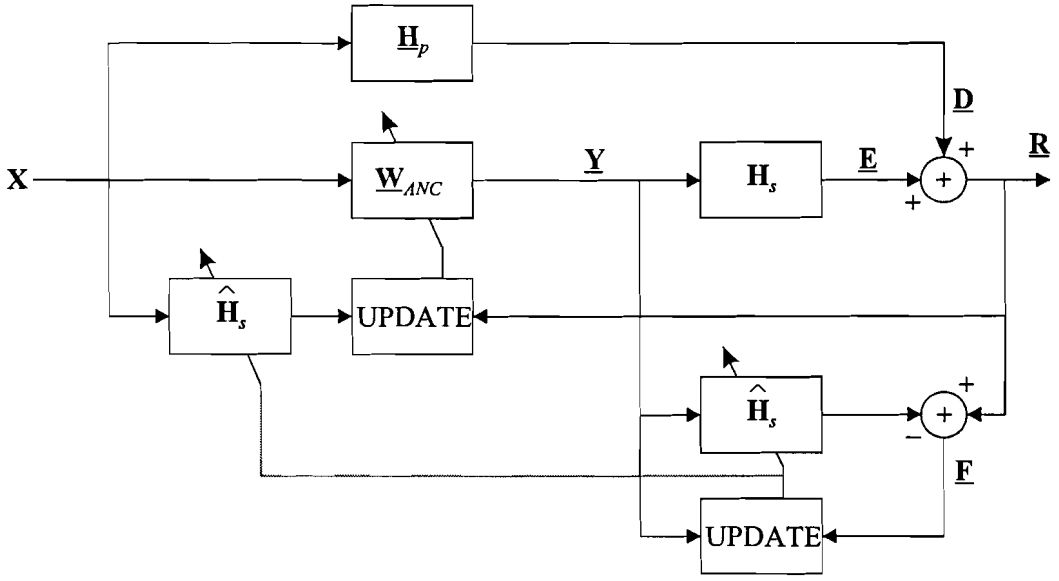

Figure 5.5. Online modeling using LMS algorithm, parallel on the secondary path.

The difference signal F can be written as:

$$\underline{\mathbf{F}} = \underline{\mathbf{R}} - \hat{\mathbf{H}}_s \cdot \underline{\mathbf{Y}} = \mathbf{X} \cdot \left\{ \underline{\mathbf{H}}_p + \mathbf{H}_s \cdot \underline{\mathbf{W}}_{ANC} - \hat{\mathbf{H}}_s \cdot \underline{\mathbf{W}}_{ANC} \right\} \qquad (5.1)$$

The LMS-algorithm minimizes this difference signal $E\{\underline{\mathbf{F}}' \cdot \underline{\mathbf{F}}\}$. Minimizing this leads to the steady state solution:

$$\hat{\mathbf{H}}_s \approx \mathbf{H}_s + \mathbf{H}_p / \underline{\mathbf{W}}_{ANC} \qquad (5.2)$$

This means that the optimal steady state solution $\hat{\mathbf{H}}_s = \mathbf{H}_s$ is biased by the term $\mathbf{H}_p / \underline{\mathbf{W}}_{ANC}$. The optimum steady state solution is not provided because $\underline{\mathbf{Y}}$ and $\mathbf{X}$ are correlated. This is not desired and can lead to an unstable filtered-X LMS algorithm. The optimal estimate of the secondary path is not found and therefore this method can't be used in a filtered-X LMS algorithm.

5.2.3. Online modeling of secondary path and primary

This method compensates for the biased term in equation (5.2), it uses LMS algorithms to estimate both $\mathbf{H}_s$ and $\underline{\mathbf{H}}_p$ online, figure 5.6. This method is also called the overall modeling method [7].

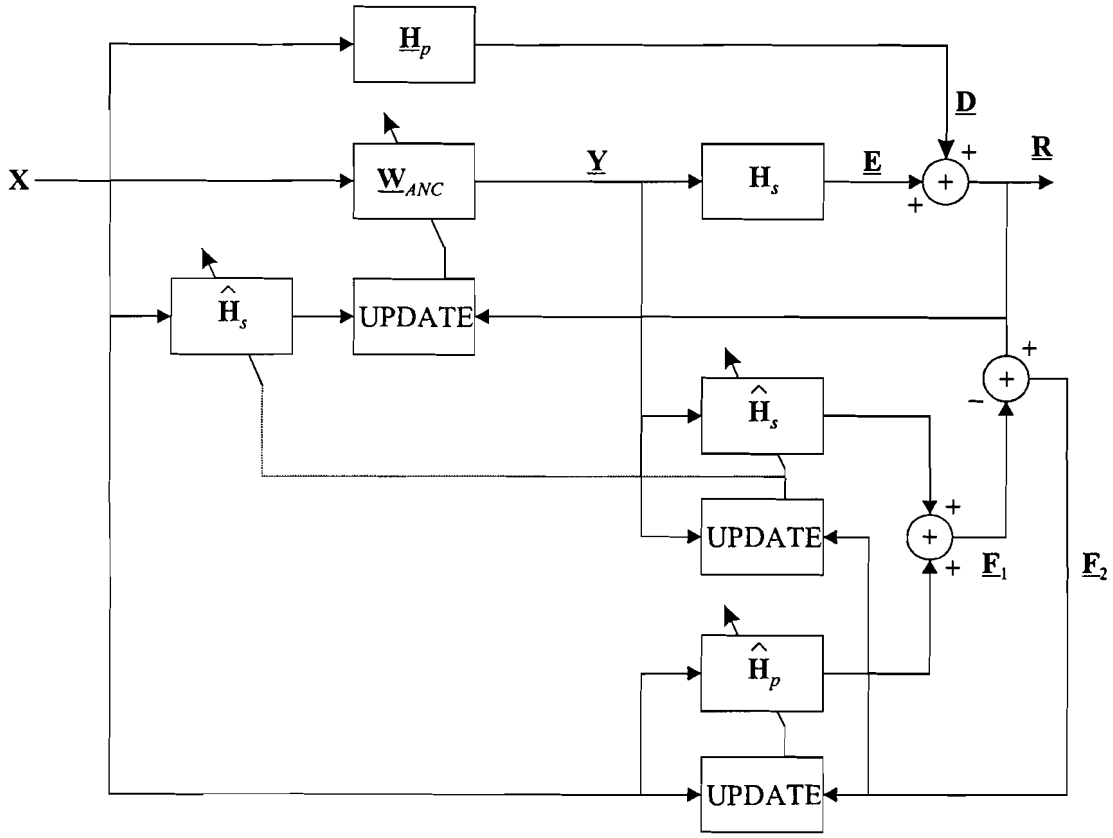

Figure 5.6. Overall modeling technique

This method uses two difference signals:

$$\underline{\mathbf{F}}_1 = \mathbf{X} \cdot \left\{ \hat{\underline{\mathbf{H}}}_p + \hat{\mathbf{H}}_s \cdot \underline{\mathbf{W}}_{ANC} \right\} \tag{5.3}$$

$$\underline{\mathbf{F}}_2 = \underline{\mathbf{R}} - \underline{\mathbf{F}}_1 = \mathbf{X} \cdot \left\{ \underline{\mathbf{H}}_p + \mathbf{H}_s \cdot \underline{\mathbf{W}}_{ANC} - \left\{ \hat{\underline{\mathbf{H}}}_p + \hat{\mathbf{H}}_s \cdot \underline{\mathbf{W}}_{ANC} \right\} \right\} \tag{5.4}$$

Minimizing difference signal $\underline{\mathbf{F}}_2$ leads to the steady state solution:

$$\underline{\mathbf{H}}_p + \mathbf{H}_s \cdot \underline{\mathbf{W}}_{ANC} \approx \hat{\underline{\mathbf{H}}}_p + \hat{\mathbf{H}}_s \cdot \underline{\mathbf{W}}_{ANC} \tag{5.5}$$

This means that this method will not always provides the proper modeling results. The proper modeling results are only provided if the conditions are satisfied [7].

The advantage of this method is that there is no additional training signal necessary to obtain the unknown transfer functions $\mathbf{H}_s$ and $\underline{\mathbf{H}}_p$. However we are only interested in the modeling of the secondary path $\mathbf{H}_s$, the calculation of $\underline{\mathbf{H}}_p$ is also necessary but requires extra calculation.

A main disadvantage of this method is that if more than one secondary source is used in the ANC, simultaneously estimation of more than 1 secondary path to one specific microphone is not possible because the signals that are used for identification are correlated. This means that the use of this online modeling technique in a multipoint ANC is not preferred.

5.3. Online modeling of secondary path using additive noise

Another category of online modeling techniques is these techniques use additive signals to determine the secondary path. Because the additive signals are independent on the input signal **X** these methods can be extended to a multipoint ANC. The disadvantage compared to the overall modeling technique is that these techniques use additive noise that degrades the performance of the ANC.

The first method in presented by [17] and uses additive noise $\underline{\mathbf{N}}$ to identify the secondary path online. For the online modeling the LMS algorithm is used, see figure 5.7.

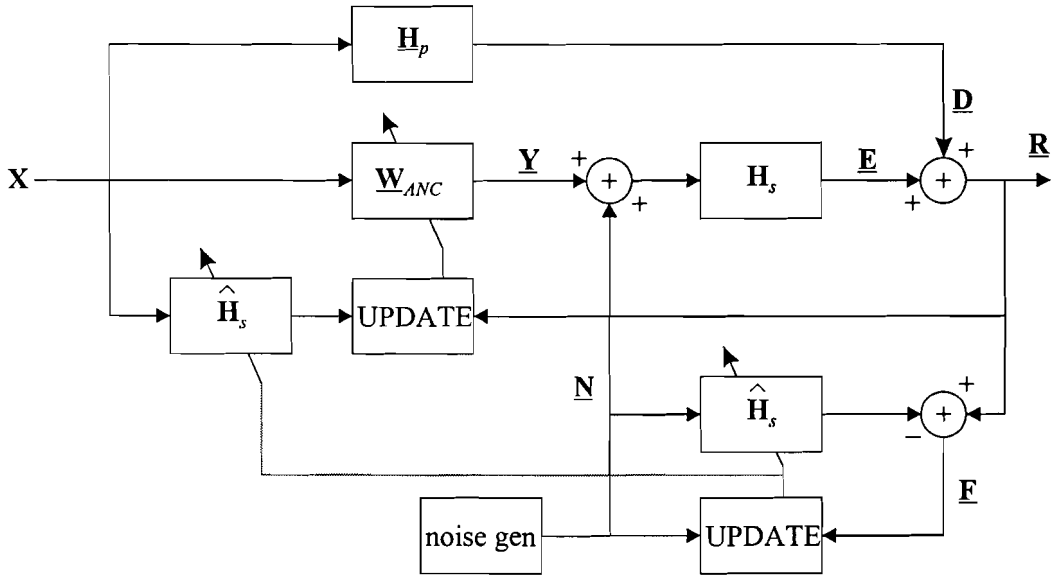

Figure 5.7. Online modeling using additive noise

For the error signal $\underline{\mathbf{R}}$ can be written:

$$\underline{\mathbf{R}} = \mathbf{X} \cdot \{\underline{\mathbf{H}}_p + \mathbf{H}_s \cdot \underline{\mathbf{W}}_{ANC}\} + \mathbf{H}_s \cdot \underline{\mathbf{N}} \qquad (5.6)$$

For the difference signal $\underline{\mathbf{F}}$ can be written:

$$\underline{\mathbf{F}} = \underline{\mathbf{R}} - \hat{\mathbf{H}}_s \cdot \underline{\mathbf{N}} = \mathbf{X} \cdot \{\underline{\mathbf{H}}_p + \mathbf{H}_s \cdot \underline{\mathbf{W}}_{ANC}\} + \mathbf{H}_s \cdot \underline{\mathbf{N}} - \hat{\mathbf{H}}_s \cdot \underline{\mathbf{N}} \qquad (5.7)$$

In the optimal steady state solution this difference signal can be approximated by $\mathbf{X} \cdot \{\underline{\mathbf{H}}_p + \mathbf{H}_s \cdot \underline{\mathbf{W}}_{ANC}\}$, because $\mathbf{H}_s \approx \hat{\mathbf{H}}_s$. This means that the adaptation process is seriously influenced by the component $\mathbf{X} \cdot \{\underline{\mathbf{H}}_p + \mathbf{H}_s \cdot \underline{\mathbf{W}}_{ANC}\}$. For stable convergence the adaptation constant for the online modeling of the secondary path has to be small and thus decreases the adaptation speed of this online modeling. Slow online modeling of the secondary path means slow convergence speed of the ANC and is not desired.

5.3.1. Enhanced method for online modeling of the secondary path using additive noise

An enhanced method that decreases the influence of the component $\mathbf{X}\cdot\{\underline{\mathbf{H}}_p+\mathbf{H}_s\cdot\underline{\mathbf{W}}_{ANC}\}$ in the adaptation of the secondary path is presented [13]. This method estimates the component $\mathbf{X}\cdot\{\underline{\mathbf{H}}_p+\mathbf{H}_s\cdot\underline{\mathbf{W}}_{ANC}\}$ using an extra LMS algorithm and therefore increases the adaptation speed significantly, see figure 5.8.

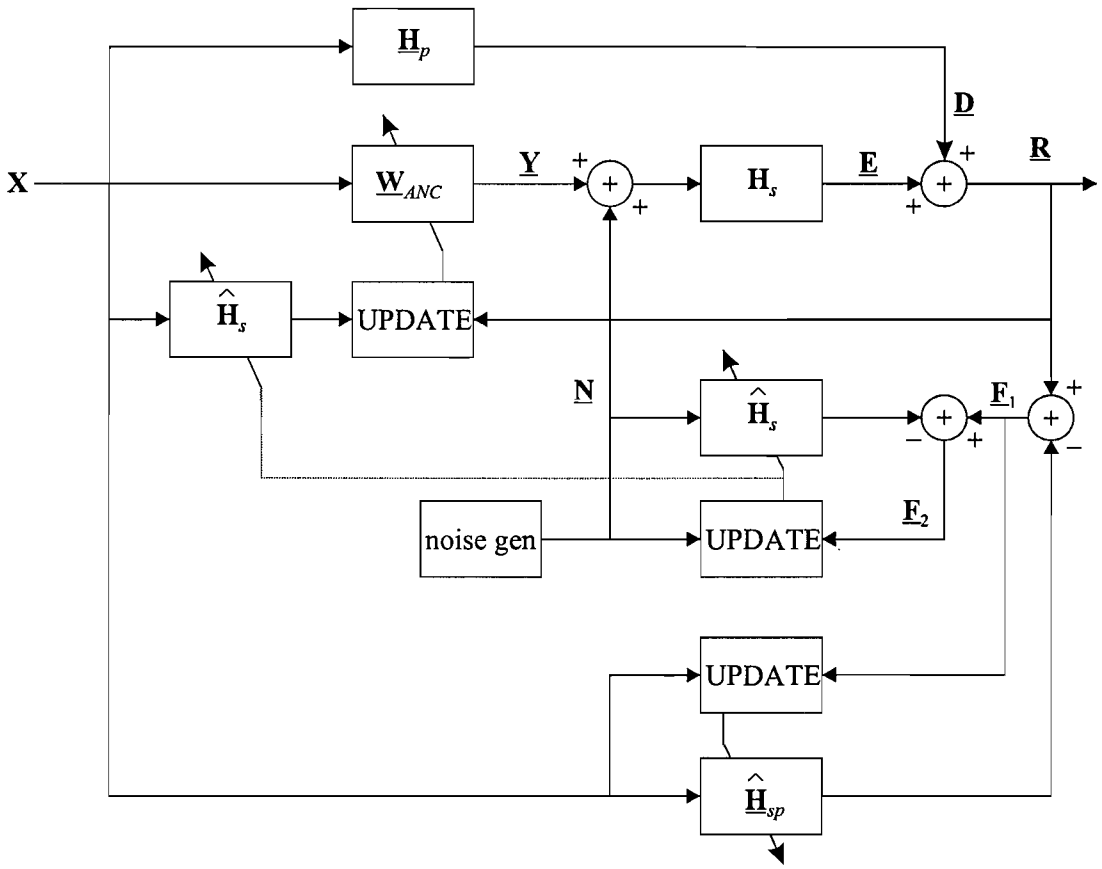

Figure 5.8. Enhanced online modeling using additive noise

For the difference signals can be written:

$$\mathbf{F}_1=\mathbf{R}-\mathbf{X}\cdot\mathbf{H}_{ps}=\mathbf{X}\cdot\{\mathbf{H}_p+\mathbf{H}_s\cdot\underline{\mathbf{W}}_{ANC}\}-\mathbf{X}\cdot\mathbf{H}_{ps}+\mathbf{H}_s\cdot\underline{\mathbf{N}} \tag{5.8}$$

$$\mathbf{F}_2=\mathbf{F}_1-\hat{\mathbf{H}}_s\cdot\underline{\mathbf{N}}=\mathbf{X}\cdot\{\mathbf{H}_p+\mathbf{H}_s\cdot\underline{\mathbf{W}}_{ANC}\}-\mathbf{X}\cdot\mathbf{H}_{ps}+\mathbf{H}_s\cdot\underline{\mathbf{N}}-\hat{\mathbf{H}}_s\cdot\underline{\mathbf{N}} \tag{5.9}$$

Minimizing $E\{\underline{\mathbf{F}}_2^t\cdot\underline{\mathbf{F}}_2\}$ leads to the optimal steady state results:

$$\mathbf{H}_p+\mathbf{H}_s\cdot\underline{\mathbf{W}}_{ANC}\approx\mathbf{H}_{ps} \tag{5.10}$$

$$\mathbf{H}_s\approx\hat{\mathbf{H}}_s \tag{5.11}$$

If equation 5.10 is satisfied the modeling of $\mathbf{H}_s$ is not disturbed by $\mathbf{X}\cdot\{\underline{\mathbf{H}}_p+\mathbf{H}_s\cdot\underline{\mathbf{W}}_{ANC}\}$. This means that the adaptation of $\mathbf{H}_s$ can be much increased and is only possible if the LMS method that is used to obtain $\underline{\mathbf{H}}_{ps}$ converges fast. The overall convergence of the modeling of the secondary path is increased

using this method, compared to the other technique. A negative aspect however is that the maximal attenuation of the ANC is limited by the additive noise required for the online modeling.

A simple simulation will show the properties of this method. For 2 different positions of the microphone the acoustical transfer functions, $\underline{\mathbf{H}}_p$ and $\mathbf{H}_s$ are identified. Figure 5.9a shows a simulation with the optimal ANC, this means $\hat{\mathbf{H}}_s = \mathbf{H}_s$. After 64 seconds the microphone is replaced, resulting in new acoustical transfer functions $\mathbf{H}_s$ and $\underline{\mathbf{H}}_p$. For the optimal ANC still holds that $\hat{\mathbf{H}}_s = \mathbf{H}_s$. Second the online modeling of the secondary path using adaptive noise is simulated, see figure 5.9b. Both methods use the same adaptation constant for the update of the ANC.

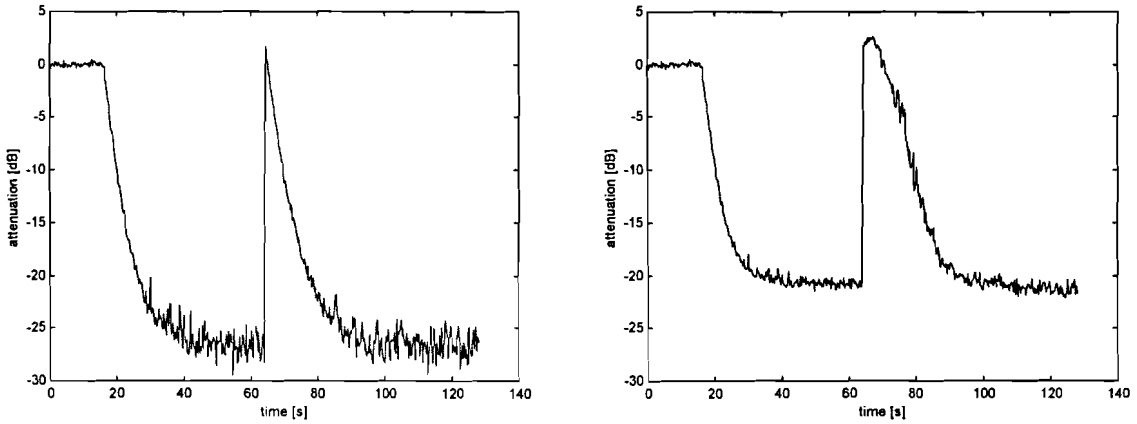

Figure 5.9. The optimal ANC (a) and the ANC with online modeling of the secondary path (b)

The additive noise limits the maximal attenuation of the ACN and this online modeling technique decreases the adaptation speed of the ANC. It is possible to decrease the additive noise but this also decreases the convergence speed of the online modeling.

5.3.2. New online modeling technique using additive noise dependent on $\underline{\mathbf{R}}$

In this section a new method is proposed that is based on the algorithm presented in the previous section but uses additional noise that is dependent on the error signal $\underline{\mathbf{R}}$. Only in those frequency-bins where the error signal is high more additional noise is used to model the secondary path. A relatively high error signal often indicates a relatively high phase error for those frequency-bins. However if the secondary path is described accurate and the ANC performs well no additional noise signal is necessary to estimate the secondary path.

Multiplying the additional noise $\underline{\mathbf{N}}_1$ elements-wise with $\underline{\mathbf{R}}$ does this:

$$\underline{\mathbf{N}}_2 = \underline{\mathbf{N}}_1 \otimes \underline{\mathbf{R}} \qquad (5.12)$$

This leads to figure 5.10.

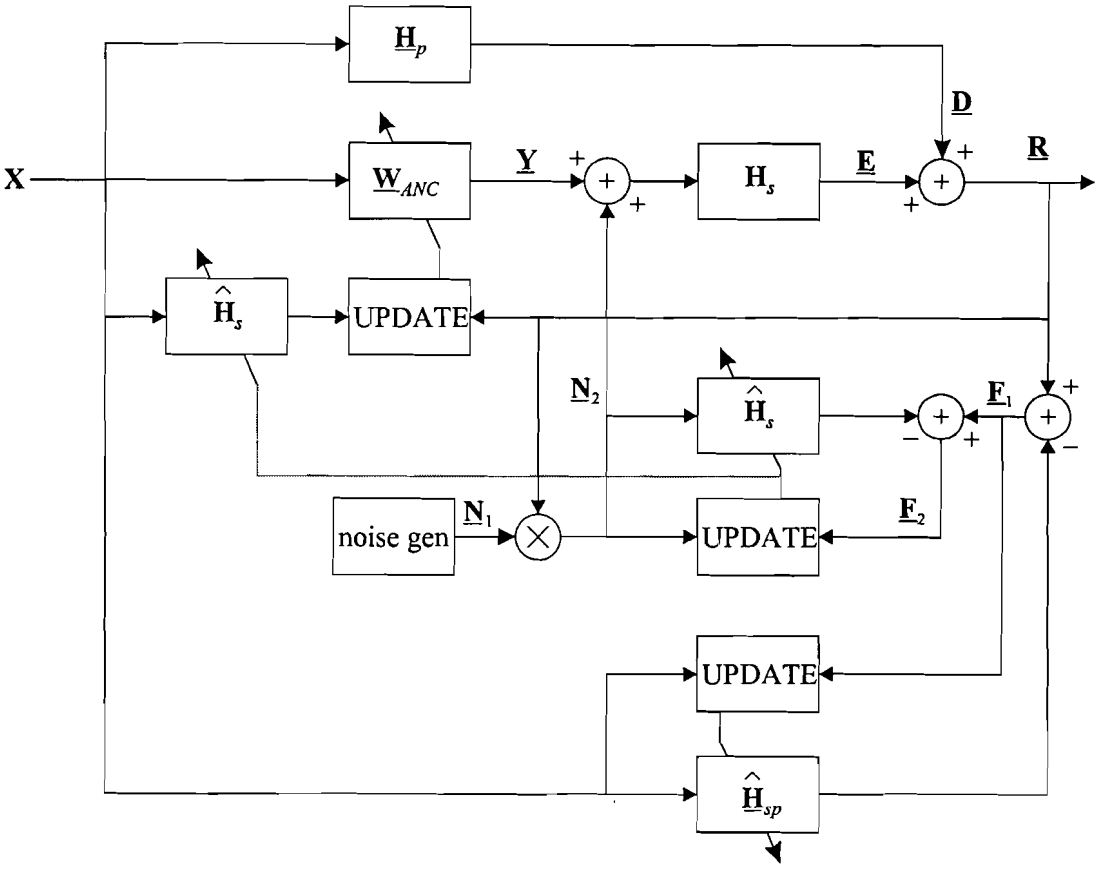

Figure 5.10. New online modeling technique using additive noise multiplied by error signal

A simple simulation will show the advantage of this method compared to the method mentioned in section 5.3.1. The simulation conditions are equal. Figure 5.11a shows a simulation with the optimal ANC, this means that $\hat{\mathbf{H}}_s = \mathbf{H}_s$. Secondly, the new online modeling technique of the secondary path is used, see figure 5.11b. Both methods use the same adaptation constant for the update of the ANC.

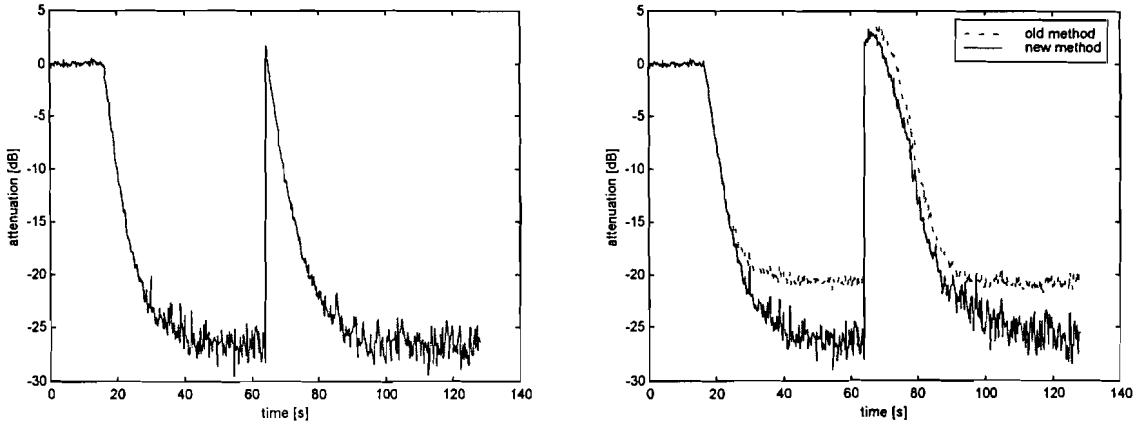

a b

Figure 5.11. The optimal ANC (a) and the ANC with online modeling of the secondary path (b)

Because the additional noise is dependent on **R** more additional noise is added if the system is initiated and less noise is added if the ANC converges. This leads to a faster adaptation speed of the secondary

path modeling. The final attenuation of the ANC increases and the maximal attenuation are comparable to the maximal attenuation of the optimal ANC.

5.4. Conclusions

In this chapter several online modeling techniques are described. The techniques can be divided into 2 classes. First the modeling techniques that use no additional training signal to model the secondary path, these methods do not degrade the performance of the ANC but can not be used in a multipoint acoustic noise canceling system because the signals used for modeling are correlated. The other methods use an additional noise signal to model the secondary path online. These methods can degrade the performance of the ANC, but can be used in a multipoint ANC and are therefor more interesting.

Current additive noise techniques degrade the maximal attenuation of the ANC and decrease the adaptation of the ANC. The new proposed method converges with increased speed compared to the current techniques and the maximal attenuation is equal to the maximal attenuation with an optimal ANC. This new method will be presented at the Prorisc '99 conference [22].

6. Conclusions

The ANC uses the filtered-X algorithm because there exists an acoustic transfer function in the control path. To ensure stable convergence the filtered-X LMS algorithm requires an accurate estimate of this acoustical path: the estimate of the acoustical path has to be within 90 degrees for every frequency-bin. In this report it is shown that the reverberation and the secondary path characteristics degrade the performance of the ANC. The performance increases if the number of loudspeakers exceeds the number of microphones.

The remaining reverberation limits the maximal attenuation of the ACN because this remaining reverberation can not be cancelled. If more sound absorbing materials are used the room acoustics change and the reverberation decreases while the maximal attenuation increases.

The frequency spectrum of the secondary path contains frequency-bins where power is relatively low. At these frequency-bins the adaptation speed is slower and lead to a larger computational error so that the final attenuation also decreases. However if the number of loudspeakers is higher than the number of microphones, the extra secondary paths can compensate for these frequency-bins and the performance increases significantly. This is only possible if the secondary paths don't have common frequency-bins where the power is low.

If the secondary path or room acoustics change, online estimation of the secondary path becomes desirable for stable filtered-X LMS algorithm. In this report several techniques for online modeling are discussed and a new method is proposed. This new method uses additive noise to estimate the secondary path online. This noise is added in each frequency-bin separately such that the noise signal does not distort the performance of the ANC. Simulations show that this new method increases the speed of convergence and the maximal attenuation compared to other additive noise algorithms.

The adaptation process of the filtered-X LMS algorithm is influenced by the estimate of the secondary path and the input signal statistics. Therefore two algorithms are discussed. First the decorrelated filtered-X LMS algorithm decorrelates the input signal such that the adaptation process is not influenced by the input signal statistics. Secondly the All-pass filtered-X LMS algorithm is introduced to make the adaptation speed independent on the secondary path characteristics. Both methods increase the adaptation speed significantly but do not lead to a higher attenuation.

7. Future research

In the last chapters the 1-1 input-output ANC was extended to a multipoint ANC. The 1-2 input-output noise canceller provides significantly more attenuation compared to the 1-1 input-output ANC. In general it means that if the number of loudspeakers exceeds the number of cancellation points the maximal attenuation increases significantly. If the 2-2 input-output ANC is extended to a 2-3 input-output ANC this will increase the maximal attenuation.

The 2-2 input-output ANC is build and will be extended to a virtual sound source generator (chapter 1). If the relation between the quality of a virtual sound source and the ANC is investigated it will become clear how much attenuation is necessary to create a virtual sound source. If this attenuation is not realizable using 2 loudspeakers the number of loudspeakers has to increase.

The new method to model the secondary path online is promising but has to be researched thoroughly, especially the relation between the adaptation constants and the online modeling.

Bibliography

[1] Garas, J. and P.C.W. Sommen

The all-pass filtered-x algorithm.
Proc. of the ninth European Signal Processing Conference, Vol. I, Rhodos, Greece, Sept. 8-11 1998, pp. 101-104

[2] Sommen, P.C.W. and J. Garas

Using phase information to decorrelate the filtered-x algorithm.
Proc. of the Int. Conf. of Acoustics, Speech and Signal Processing conf., May 12-15, 1998, Seattle USA, pp. 1397-1400

[3] Chen, G. and T. Sone

The stability and convergence characteristics of the delayed-x LMS algorithm in ANC systems
Journal of Sound and Vibration, Vol. 216, No. 4, 1998, pp. 637-648

[4] Schobben, D.W.E. and P.C.W. Sommen

On the performance of too short adaptive filters.
Proceedings of the ProRISC Workshop on Circuits, Systems nd Signal Processing, 1997, p. 545-549

[5] Mathijssen, A.W.M.

Generation of phantom sound sources with Block Frequency Domain Adaptive Filtering.
Master thesis, publ. by Eindhoven University of Technology, Department of Signal processing, 1997

[6] Chen, G. and M. Abe, T. Sone

Improvement of the convergence characteristics of the ANC system with the LMS algorithm by reducing the effect of secondary paths.
Journal of the Acoustical Society of Japan (E), Vol. 17, No. 6, 1996, pp. 295-303

[7] Saito, N. and T. Sone, T. Ise and M. Akiho

Optimal on-line modeling of primary and secondary paths in active noise control systems,
Journal of the Acoustical Society of Japan (E), Vol. 17, No. 6, 1996, pp. 275-283

[8] Chen, G. and M. Abe, T. Sone

Effects of multiple secondary paths on convergence properties in active noise control systems with LMS algorithm.
Journal of Sound and Vibration, Vol. 195, No. 2, 1996, pp. 217-228

[9] Haiyan He

Real-time generation of phantom sound sources in a large frequency range.
Stan Ackermans Institute Report, Eindhoven, 1996, ISBN 90-5282-652-8

[10] Tol, F.J.C. van der

Creation of phantom sources using adaptive filters.
Master thesis, publ. of the Eindhoven University of Technology, Electronic Circuit Design Group, Eindhoven, 1995

[11] Chen, G. and M. Abe, T. Sone

Evaluation of the convergence characteristics of the filtered-X LMS algorithm in the frequency domain.
Journal of the Acoustical Society of Japan, Vol 16 (1995), No. 6, p. 331-340

[12] Snyder, S.D. and C.H. Hansen

The effect of transfer function estimation errors on the filtered-X LMS algorithm.
IEEE Transactions on signal processing, Vol. 42, No. 4, April 1994, pp. 950-953

[13] Bao, C. and P. Sas, H. Van Brussel

Adaptive active control of noise in 3-D reverberant enclosures
Journal of sound and vibration, Vol. 161, 1993, p. 501-514

[14] Nelson, P.A. and H. Hamada, S.J. Elliott

Adaptive inverse filters for stereophonic sound reproduction.
IEEE transactions on signal processing, Vol., 40, No. 7, July 1992, pp. 1621-1632

[15] Sommen, P.C.W.

Adaptive filtering methods.
Ph. D. thesis, Eindhoven University of Technology, The Netherlands, June 1992, ISBN 90-9005143-0

[16] Boucher, C.C. and S.J. Elliott, P.A. Nelson

Effect of errors in the plant model on the performace of algorithms for adaptive feedforward control.
IEE Proceedings-F, Vol. 138, No. 4, August 1991, pp. 313-319

[17] Eriksson, L.J. and M.C. Allie

Use of random noise for on-line transducer modeling in an adptive active attenuation system
Journal of the Acoustical Society of America, Vol. 85(1989), p. 797-802

[18] Masato Miyoshi and Yutaka Kaneda

Inverse filtering of room acoustics.
IEEE transactions on acoustics, speech and signal processing, Vol. 36, No. 2, February 1988, pp. 145-152

[19] Elliott, S.J. and I.A. Stothers, P.A. Nelson

A multiple error LMS algorithm and its application to the active control of sound and vibration.
IEEE transactions on Acoustics, speech and signal processing, Vol. 35, No. 10, October 1987, pp.1423-1434

[20] Widrow, B. and S.D. Stearns

Adaptive signal processing.
Prentence Hall, Inc. , Englewood Cliffs, New Jersey, 1985, ISBN 0-13-004029-0

[21] Morgan, D.R.

An analysis of multiple correlation cancellation loops with a filter in the auxiliary path.
IEEE transactions on acoustics, speech and signal processing, Vol. 28, No. 4, August 1980, pp. 454-467

[22] Cornelissen, D and P.C.W. Sommen

New online secondary path estimation in a multipoint filtered-X algorithm for acoustic noise canceling
To appear in: Prorisc 1999